Mon. Not. R. Astron. Soc. **000**, 1–20 (2000) Printed 11 July 2001 (MN LaTeX style file v1.4)

The Origin of the Density Distribution of Disk Galaxies: A New Problem for the Standard Model of Disk Formation

Frank C. van den Bosch
Max-Planck Institut für Astrophysik, Karl Schwarzschild Str. 1, Postfach 1317, 85741 Garching, Germany

ABSTRACT
We present new models for the formation of disk galaxies that improve upon previous models by following the detailed accretion and cooling of the baryonic mass, and by using realistic distributions of specific angular momentum. Under the assumption of detailed angular momentum conservation the disks that form have density distributions that are more centrally concentrated than an exponential. We examine the influence of star formation, bulge formation, and feedback on the outcome of the surface brightness distributions of the stars. Low angular momentum haloes yield disk galaxies with a significant bulge component and with a stellar disk that is close to exponential, in good agreement with observations. High angular momentum haloes, on the other hand, produce stellar disks that are much more concentrated than an exponential, in clear conflict with observations. At large radii, the models reveal distinct truncation radii in both the stars and the cold gas. The stellar truncation radii owe to our implementation of star formation threshold densities, and are in excellent agreement with observations. The truncation radii in the density distribution of the cold gas reflect the maximum specific angular momentum of the gas that has cooled. We find that these truncation radii occur at HI surface densities of roughly 1 $M_{\odot}$ pc^{-2}, in conflict with observations. We examine various modifications to our models, including feedback, viscosity, and dark matter haloes with constant density cores, but show that the models consistently fail to produce bulge-less disks with exponential surface brightness profiles. This signals a new problem for the standard model of disk formation: if the baryonic component of the protogalaxies out of which disk galaxies form have the same angular momentum distribution as the dark matter, disks are too compact.

Key words: galaxies: formation — galaxies: fundamental parameters — galaxies: spiral — galaxies: kinematics and dynamics — galaxies: structure — dark matter.

1 INTRODUCTION

In the current paradigm for galaxy formation, set forth by White & Rees (1978) and Fall & Efstathiou (1980), galaxies are considered to form through the cooling of baryons inside dark matter haloes that grow by means of gravitational instability and acquire angular momentum from cosmological torques. If the cooling baryons conserve their specific angular momentum, disk galaxies will form in the centres of the haloes, with scale lengths that are in good agreement with observations (e.g., Dalcanton, Spergel & Summers 1997; Mo, Mao & White 1998; de Jong & Lacey 2000).

However, detailed hydrodynamical simulations aimed at investigating this process of galaxy formation have indicated an important problem for the cold dark matter (CDM) model. In CDM cosmologies haloes form hierarchically by the merging of many lower mass haloes. Because the cooling in dense, low mass haloes is very efficient, the baryons in these systems have already cooled by the time they merge with the more massive protogalaxy. They reach the centre of the potential well by means of dynamical friction, through which they loose a significant fraction of their specific angular momentum to the dark matter. Consequently, the disks that form in these simulations are an order of magnitude too small (Navarro & Benz 1991; White & Navarro 1993; Navarro & Steinmetz 1999). This has become known as the *angular momentum catastrophe* of disk galaxy formation.

Several solutions to this problem have been suggested. Weil, Eke & Efstathiou (1998), Domínguez-Tenreiro, Tissera & Sáiz (1998), Sommer-Larsen, Gelato & Vedel (1999) and Eke, Efstathiou & Wright (2000) argued that stellar feedback and/or ionizing background radiation can prevent the cooling of gas in these small mass haloes, therewith considerably reducing the angular momentum loss (but see Navarro & Steinmetz 1997). An alternative suggestion has been to alter the power spectrum of initial density fluctuations, either by invoking an alternative form of dark matter (Sommer-Larsen & Dolgov 2001), or by resorting to a specific model for inflation (Kamionkowski & Liddle 2000). At the present, it is still unclear which of these solutions, if any, is most successful. What has become clear, however, is that if cosmological torques are indeed the main source of angular momentum on galactic scales, there is very little room for any angular momentum loss if we want to explain the sizes of present day disk galaxies.

Motivated by this understanding, the past couple of years a large number of studies have presented analytical models for the formation of disk galaxies that rely on the assumption of detailed angular momentum conservation. Kauffmann (1996) investigated the properties of disk galaxies within this framework, and linked it to the evolution of damped Lyα absorption systems. Dalcanton et al. (1997) and Mo et al. (1998) investigated the structural properties of disks, with emphasis on the variance induced by the distribution in halo angular momentum. Subsequent studies included recipes for bulge formation, gas viscosity, star formation and/or feedback and investigated more detailed properties of these model disk galaxies, such as the Tully-Fisher relation, the gas mass fractions, and the origin of the Hubble sequence (van den Bosch 1998, 2000; Jimenez et al. 1998; Natarajan 1999; Heavens & Jimenez 1999; van den Bosch & Dalcanton 2000; Firmani & Avila-Reese 2000; Avila-Reese & Firmani 2000; Efstathiou 2000; Zhang & Wyse 2000; Buchalter, Jimenez & Kamionkowski 2001; Ferguson & Clarke 2001).

One important shortcoming of most of these models, however, is that they make the *a priori* assumption that the cooled gas arranges itself in an exponential disk. However, one of the open issues in the formation of disk galaxies, is to actually understand why they reveal a universal surface brightness distribution. If disk galaxies indeed form as envisioned in our standard picture, their resulting density distribution is directly related to the specific angular momentum distribution of the protogalaxy. Motivated by the work of Mestel (1963) and Crampin & Hoyle (1964), Dalcanton et al. (1997) made the assumption that the protogalaxy has the angular momentum distribution of a uniform sphere in solid-body rotation, and showed that the resulting disks are actually more centrally concentrated than an exponential. Firmani & Avila-Reese (2000) used more realistic distributions of mass and angular momentum for the dark matter haloes, but again found similarly concentrated disks. Bullock et al. (2000) determined the distribution of specific angular momentum in CDM haloes from high resolution N-body simulations, and again concluded that these distributions will form overly concentrated disks. Therefore, if our picture for disk formation is correct, the question arises whether the subsequent processes of star formation, bulge formation and feedback can produce exponential stellar disks in agreement with observations.

Here we present new, but similar, models for the formation of disk galaxies. These models, presented in Section 2, will be used in forthcoming papers to investigate a wide range of disk properties such as colors and metallicities, gas mass fractions, and the Tully-Fisher relation. In this paper, however, we focus solely on the density distributions of the resulting disks. In Section 3 we investigate the effects of star formation and bulge formation on the outcome of the surface brightness profiles of the disks. In Section 4 we compare the truncation radii predicted by the models with observations. A problem with reproducing low surface brightness galaxies is discussed in Section 5, and we summarize our results in Section 6.

2 THE MODELS

2.1 The basic framework

The main assumptions that characterize the framework of our models are the following: (i) dark matter haloes around disk galaxies grow by the smooth accretion of mass, (ii) the angular momentum of protogalaxies originates from cosmological torques, (iii) in the absence of cooling the baryons have the same distribution of mass and angular momentum as the dark matter, and (iv) the cooling baryons conserve their specific angular momentum.

The two main ingredients that determine the formation and evolution of a disk galaxy, therefore, are (the evolution of) the mass and angular momentum of the virialized object; $M_{\rm vir}(r,z)$ and $J_{\rm vir}(r,z)^{\star}$. We characterize the angular momentum of the protogalaxies by the dimensionless spin parameter $\lambda = J_{\rm vir} |E_{\rm vir}|^{1/2} G^{-1} M_{\rm vir}^{-5/2}$. Here $E_{\rm vir}$ is the halo's energy, and G is the gravitational constant. We follow Firmani & Avila-Reese (2000) and make the additional assumptions that (i) the spin parameter λ of a given galaxy is constant with time, (ii) each mass shell that virializes is in solid body rotation, and (iii) the rotation axes of all shells are aligned.

None of these assumptions are necessarily accurate. For instance, the assumption of smooth mass accretion seems inconsistent with the hierarchical merger picture of structure formation in a CDM universe. On the other hand, the fragility of disks (e.g., Tóth & Ostriker 1992) suggests that mergers can not have played a dominant rôle in establishing the main properties of disk galaxies. Furthermore, numerical simulations suggest that too much merging results in disks that are too small, as baryons tend to loose their angular momentum to the dark matter in the process. The assumptions regarding the angular momentum are also questionable. Nevertheless, as we show in Section 5.5, these assumptions result in haloes with an angular momentum profile that is in good agreement with high resolution N-body simulations. Finally, we like to stress that the main goal of this study is to explore how the final disk characteristics depend on the various model ingredients. We therefore adhere to simple, parameterized descriptions of the mass accretion history (hereafter MAH) and angular momentum distribution. Although perhaps not completely realistic, they provide useful insights.

The main outline of the models is as follows. We set up a radial grid between $r = 0$ and the present day virial radius of the model galaxy and we follow the formation and evolution of the disk galaxy using a few hundred time steps. We consider six mass components: dark matter, hot gas, disk mass (both in stars and in cold gas), bulge mass, and mass

* Throughout this paper, r and z refer to spherical radius and redshift, respectively.

ejected by outflows from the disk. The dark matter, hot gas, and bulge mass are assumed to be distributed in spherical shells, whereas the disk stars and cold gas are assumed to be in infinitesimally thin annuli. Each time step we compute the changes in these various mass components in each radial bin. Below we describe the detailed prescriptions used.

2.2 The evolution of the dark matter component

The backbone of the models is the formation and evolution of the dark matter haloes, which is determined by the parameters of the background cosmological model and by the power spectrum $P(k)$ of the initial density fluctuations. The parameters of importance for the models presented here are the present day matter density Ω_0, the present day density in the form of a cosmological constant Ω_Λ, the Hubble constant $h \equiv H_0/(100\,\mathrm{km\,s^{-1}\,Mpc^{-1}})$, the baryon density $\Omega_{\rm bar}$, and the normalization σ_8 of $P(k)$.

As discussed above, we make the assumption that protogalaxies accrete mass smoothly. Rather than attempting to link the actual accretion rate to the cosmological framework, using for instance the extended Press-Schechter formalism to construct merger histories, we adopt a simple parameterization. This has the advantage that we can describe the mass accretion history (hereafter MAH) by one or two free parameters.

For a given virialized mass at $z = 0$, $M_{\rm vir}(0)$, we write the MAH as

$$M_{\rm vir}(z) = M_{\rm vir}(0)\left[1 - \frac{\log(1+z)}{\log(1+z_f)}\right]^{1/a} \tag{1}$$

Here a and z_f are free parameters. The parameter a describes whether most of the final virial mass is accreted early or late. In Figure 1 we plot MAHs for $z_f = 10$ and three different values of a: 0.3, 0.6 and 0.9. The corresponding redshifts at which half the present day mass is assembled are 0.57, 1.26, and 2.04, respectively. A comparison with MAHs computed using the extended Press-Schechter approximation based on the conditional probabilities for a Gaussian random field shows that the parameterization (1) with $z_f = 10$ and $0.3 \lesssim a \lesssim 0.9$ comprises ~ 95 percent of the typical MAHs for a typical galaxy sized halo, with $a = 0.6$ close to the average (cf. Lacey & Cole 1993; Firmani & Avila-Reese 2000; Buchalter et al. 2001). Clearly, in reality the values of z_f and a will depend on the mass of the object. This is not taken into account here. The aim of this paper is not to use the most accurate MAHs, but merely to use a simple parameterization to investigate how the resulting disk surface densities depend on the MAH. Therefore, in what follows, we use values of a in the range 0.3-0.9 (with z_f fixed at 10) to gauge the dependence of our models on the MAHs. When required, we shall explore a wider range of z_f and a values.

The virial radius of dark matter haloes as function of redshift is given by

$$r_{\rm vir}(z) = 169.0\,h^{-1}\,\mathrm{kpc}\left(\frac{M_{\rm vir}(z)}{10^{12}h^{-1}\,\mathrm{M}_\odot}\right)^{1/3}\left(\frac{\Omega(z)}{\Omega_0}\right)^{1/3} \left(\frac{\Delta_{\rm vir}(z)}{178}\right)^{-1/3}(1+z)^{-1} \tag{2}$$

with $\Delta_{\rm vir}$ the virial density, defined as the average density

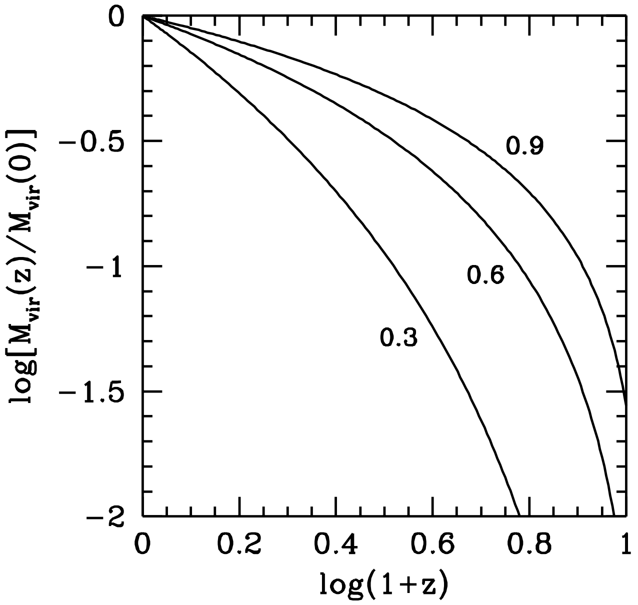

Figure 1. The mass accretion histories (MAHs) defined by equation (1) for $z_f = 10$ and three different values of a. These curves describe the growth of halo mass, normalized to the present day mass, as function of redshift. A comparison with Figure 1 in Firmani & Avila-Reese (2000) shows that these MAHs are in reasonable agreement with the 5, 50, and 95 percentile MAHs computed using the extended Press-Schechter approximation.

inside $r_{\rm vir}$ expressed in terms of the critical density for closure. We use the fitting formula of Bryan & Norman (1998):

$$\Delta_{\rm vir}(z) = 18\pi^2 + 82x - 39x^2 \tag{3}$$

with $x = \Omega(z) - 1$. This fitting formula is valid for a flat Universe ($\Omega_0 + \Omega_\Lambda = 1$) and accurate to one percent in the range $0.1 \leq \Omega(z) \leq 1.0$.

Rather than attempting to compute the density distribution of virialized haloes from extended secondary infall models, as for instance in Avila-Reese, Firmani & Hernández (1998), we adopt a simple parameterized density distribution. We assume that the dark matter virializes such that at each redshift the halo's density distribution is given by

$$\rho_{\rm vir}(r) = \rho_s\left(\frac{r}{r_s}\right)^{-\gamma}\left(1 + \frac{r}{r_s}\right)^{\gamma-3} \tag{4}$$

with ρ_s and r_s dependent on z and $M_{\rm vir}(z)$. This profile is motivated by both numerical simulations and by the observed rotation curves of disk galaxies: numerical simulations of structure formation in a CDM universe suggest values for γ in the range $1.0-1.5$ (e.g., Navarro, Frenk & White 1996, 1997; Fukushige & Makino 1997; Moore et al. 1998), whereas rotation curves of disk galaxies imply $0 \leq \gamma \lesssim 1.5$ (van den Bosch et al. 2000; van den Bosch & Swaters 2001). We mainly focus on models with $\gamma = 1$ for which equation (4) reduces to the NFW profile (Navarro, Frenk & White 1997). However, because of the relatively large uncertainties we shall also consider other values of γ.

The total mass, energy, and angular momentum of a halo with density distribution (4) are given by:

$$M_{\rm vir} = 4\pi\rho_s r_s^3 f(c), \tag{5}$$

$$E_{\rm vir} = -\frac{1}{2} M_{\rm vir} V_{\rm vir}^2 f(c)^{-2} h(c), \tag{6}$$

and

$$J_{\rm vir} = \sqrt{2}\, \lambda\, r_{\rm vir} M_{\rm vir} V_{\rm vir} f(c) h(c)^{-1/2}. \tag{7}$$

Here $V_{\rm vir}$ is the circular velocity of the halo at the virial radius, $c = r_{\rm vir}/r_s$ is the halo concentration parameter, and $f(x)$ and $h(x)$ are given by

$$f(x) = \int_0^x {\rm d}y\, y^{2-\gamma} (1+y)^{\gamma-3}, \tag{8}$$

and

$$h(x) = x \int_0^x {\rm d}y\, f(y)\, y^{1-\gamma} (1+y)^{\gamma-3}, \tag{9}$$

Equations (1)–(5) completely specify the dark matter density distribution at each redshift once we know the value of the concentration parameter c as function of z. We use the model of Bullock et al. (2001), which gives

$$c(M_{\rm vir}, z) = C_0 \left(\frac{1+z_{\rm coll}}{1+z} \right) \tag{10}$$

with $z_{\rm coll}$ the redshift at which a mass $f \cdot M_{\rm vir}$ collapses. Here C_0 and f are constants that depend on the cosmology.

Note that in our approach all haloes at the same redshift and with the same mass have the same concentration parameter c. However, in reality there is a large spread in values of c (e.g., Jing 2000; Bullock et al. 2001). Furthermore one expects that c is correlated with the actual MAHs, such that MAHs with a higher value of a (i.e., more early accretion) are more concentrated (e.g., Avila-Reese, Firmani & Hernández 1998; Firmani & Avila-Reese 2000). We ignore this scatter in c and its associated correlation with a. Despite these obvious shortcomings, the simplicity of the above parameterizations allows us to investigate the main dependencies of our models, which is our main concern in this paper.

Numerous studies, both analytical and numerical, have shown that the distribution of the spin parameter λ is well described by a log-normal distribution

$$p(\lambda){\rm d}\lambda = \frac{1}{\sigma_\lambda \sqrt{2\pi}} \exp\left(-\frac{\ln^2(\lambda/\bar{\lambda})}{2\sigma_\lambda^2} \right) \frac{{\rm d}\lambda}{\lambda}, \tag{11}$$

(e.g., Barnes & Efstathiou 1987; Ryden 1988; Cole & Lacey 1996; Warren et al. 1992). In this paper we gauge the λ-dependence of our models by constructing models with $\lambda =$ 0.028, 0.06, and 0.129. These values correspond to the 10, 50, and 90 percentile points of the distribution of equation (11) with $\bar{\lambda} = 0.06$ and $\sigma_\lambda = 0.6$.

2.3 Disk formation

In order to compute the formation and evolution of the disks we proceed as follows. Each time step Δt a shell with mass $\Delta M = M_{\rm vir}(t) - M_{\rm vir}(t - \Delta t)$ virializes. A fraction $f_{\rm bar} = \Omega_{\rm bar}/\Omega_0$ of this mass is in baryons, and is heated to the halo's virial temperature

$$T_{\rm vir} = \frac{1}{2} \frac{\mu m_{\rm p}}{k} V_{\rm vir}^2 \tag{12}$$

where $\mu m_{\rm p}$ is the mass per particle, and k is Boltzmann's constant. This gas is added to the hot gas component between radii $r_{\rm min}$ and $r_{\rm max}$, whereby we assume that the gas follows the same density distribution as the dark matter. Assuming no shell crossing we add ΔM to the outer parts of the halo, and we thus set $r_{\rm max}$ equal to the virial radius at t, and $r_{\rm min}$ to the radius inside of which the total mass (baryons plus dark matter) is equal to the virial mass at time $t - \Delta t$. The baryons dissipate energy radiatively, but are assumed to conserve their specific angular momentum. The time scale on which they will reach centrifugal equilibrium in the disk is given by $t_c \equiv \max[t_{\rm ff}, t_{\rm cool}]$. Here $t_{\rm ff}$ is the free-fall time defined as

$$t_{\rm ff} = \sqrt{\frac{3\pi}{32 G \bar{\rho}}}, \tag{13}$$

with $\bar{\rho}$ the average halo density, and

$$t_{\rm cool} = \frac{3}{2} \mu m_{\rm p} \frac{k T_{\rm vir}}{\rho_{\rm gas} \Lambda_N(Z_{\rm hot})} \frac{\mu_e^2}{\mu_e - 1} \tag{14}$$

is the cooling time. Here μ_e is the number of particles per electron, and $\Lambda_N(Z_{\rm hot})$ is the normalized cooling function for a gas with metallicity $Z_{\rm hot}$. For Λ_N we use the collisional ionization equilibrium cooling functions of Sutherland & Dopita (1993), assuming a Helium mass abundance of 0.25.

Within our framework outlined in Section 2.1, the radius at which the baryons reach centrifugal equilibrium is computed as follows. For a shell with $r_{\rm min} < r < r_{\rm max}$ in solid body rotation with circular frequency ω_0 and with density distribution $\rho(r)$ the total angular momentum is given by

$$J_{\rm shell} = \frac{8}{3}\, \pi\, \omega_0 \int_{r_{\rm min}}^{r_{\rm max}} {\rm d}r\; r^4\; \rho(r) \tag{15}$$

One can also write the angular momentum of the shell as $\Delta J \equiv J_{\rm vir}(t) - J_{\rm vir}(t - \Delta t)$, i.e., the difference in the total angular momentum of the halo before and after the addition of the new shell of matter. Here $J_{\rm vir}(t)$ is given by equation (7). Thus, for the shell's circular frequency one finds

$$\omega_0 = \frac{3}{8\pi}\, \Delta J \left[\int_{r_{\rm min}}^{r_{\rm max}} {\rm d}r\; r^4\; \rho(r) \right]^{-1} \tag{16}$$

At time $t' = t + t_c$ we add these baryons to the disk. Using detailed conservation of specific angular momentum, we compute the baryonic mass added to the disk annulus with $r_k < r \leq r_{k+1}$ as the baryonic shell mass with cylindrical radii $R_k < R \leq R_{k+1}$. Here

$$R_i = \sqrt{\frac{r_i\, V_c(r_i, t')}{\omega_0}} \tag{17}$$

with $V_c(r_i, t')$ the total circular velocity of the galaxy at radius r_i at time t'. Throughout we assume that the disk is infinitesimally thin, and each time step we use the adiabatic invariant formalism of Blumenthal et al. (1986) and Flores et al. (1993) to compute the gravitational contraction of the dark matter induced by the baryons settling in the disk.

2.4 Star formation

Star formation in (disk) galaxies is a complicated process which is only poorly understood. In particular, it is unclear whether, in isolated disk galaxies, star formation is mainly triggered by density waves (Wyse 1986; Wyse & Silk 1989), by local feedback from supernovae (Gerola & Seiden 1978), or by cloud-cloud interactions (Tan 2000). Furthermore, although it is generally accepted that the star formation is self-regulated, the detailed interplay between gravitational instabilities, supernovae feedback, turbulent viscosity, magnetic fields, and star formation is still heavily debated (see e.g., Firmani & Tutukov 1994; Silk 1997; Tan 2000; and references therein). Therefore, we use a star formation recipe that is motivated by empirical findings, so that despite our ignorance, we are implicitly taking account of all these detailed physical processes.

Observations have shown that the star formation rates in disk galaxies are well fit by a simple Schmidt (1959) law:

$$\psi = \varepsilon_{\rm SF}\,\Sigma_{\rm gas}^{n} \tag{18}$$

This simple empirical law holds over many orders of magnitude in gas surface density, and even applies to circumnuclear starburst regions. However, when applied to *local* gas densities, the Schmidt law breaks down at large disk radii, where the star formation is found to be abruptly suppressed. In a seminal paper, Kennicutt (1989) showed that these radii correspond to the radii where the gas surface density falls below the critical surface density given by Toomre's (1964) stability criterion:

$$\Sigma_{\rm crit}(R) = \frac{\sigma_{\rm gas}\,\kappa(R)}{3.36\,G\,Q}. \tag{19}$$

Here Q is a dimensionless constant near unity, $\sigma_{\rm gas}$ is the velocity dispersion of the gas, and κ is the epicycle frequency given by

$$\kappa(R) = \sqrt{2}\,\frac{V_c(R)}{R}\left(1 + \frac{R}{V_c(R)}\frac{{\rm d}V_c}{{\rm d}R}\right)^{1/2}. \tag{20}$$

with $V_c(r)$ the circular velocity of the entire system.

Solving ${\rm d}\Sigma_{\rm gas}/{\rm d}t = -\psi$, yields

$$\Sigma_{\rm gas}(t) = \left[-\frac{\varepsilon_{\rm SF}}{m}\Delta t + \Sigma_{\rm gas}^{1/m}(t-\Delta t)\right]^{m} \tag{21}$$

with $m = 1/(1-n)$ (cf. Heavens & Jimenez 1999). In each annulus in the disk we then compute the mass in stars formed between $t-\Delta t$ and t as

$$\Delta M_{*} = A\left[\Sigma_{\rm gas}(t-\Delta t) - \tilde{\Sigma}_{\rm gas}(t)\right], \tag{22}$$

with A the area of the annulus and $\tilde{\Sigma}_{\rm gas}(t) = \max[\Sigma_{\rm crit}(t), \Sigma_{\rm gas}(t)]$. This way, star formation is not allowed to deplete gas to surface densities below $\Sigma_{\rm crit}$.

2.5 Feedback by Supernovae

When stars evolve they put energy into the interstellar medium (ISM) which impacts on the further evolution of the galaxy. By resorting to an empirical description of the star formation, we are implicitly taking account of the effects that these feedback processes have on the star formation rate. What is not taken into account, however, is a possible feedback-driven outflow of gas from the disk. Here we use a simple parametric model, similar to the ones used in various semi-analytical models for galaxy formation. We assume that the amount of gas blown out of the disk is proportional to the total energy input by supernovae (SNe) and inversely proportional to the escape velocity squared. At each time step we compute the total energy injected into the ISM at each disk annulus as

$$E = \eta_{\rm SN}\,\Delta M_{*}\,E_{\rm SN} \tag{23}$$

Here ΔM_{*} is the mass in stars formed (equation [22]), $E_{\rm SN} = 10^{51}$ergs is the energy produced by one SN, and $\eta_{\rm SN}$ is the number of SNe per solar mass of stars formed. We assume that this energy drives a galactic wind, whereby a mass $\Delta M_{\rm eject}$ is blown out of the halo. Requiring energy balance one obtains

$$\Delta M_{\rm eject} = \frac{2\,\varepsilon_{\rm fb}\,\eta_{\rm SN}\,E_{\rm SN}}{V_{\rm esc}^2}\,\Delta M_{*} \tag{24}$$

(cf. Kauffmann, White & Guiderdoni 1993; Natarajan 1999). Here $V_{\rm esc}$ is the local escape velocity, and $\varepsilon_{\rm fb}$ is a free parameter that describes what fraction of the energy released by SNe is converted into kinetic energy to drive the outflow. For simplicity, we assume that the ejected mass is forever lost from the system: the ejected mass is not considered for later infall, and the corresponding metals are not used to enrich the infalling gas.

2.6 Bulge formation

Self-gravitating disks tend to be unstable against global instabilities such as bar formation. Here we follow the approach of van den Bosch (1998, 2000) and Avila-Reese & Firmani (2000) and assume that an unstable disk transforms part of its disk material into a bulge component in a self-regulating fashion such that the final disk is marginally stable.

Motivated by the work of Christodoulou, Shlosman & Tohline (1995) we consider a disk to be unstable if

$$\alpha_{\rm max} = \max_{0\leq r\leq r_{\rm vir}}\left(\frac{V_{\rm disk}(r)}{V_{\rm circ}(r)}\right) < \alpha_{\rm crit}. \tag{25}$$

Here $\alpha_{\rm crit}$ is a free parameter, which regulates the disk-to-bulge ratios of the final model galaxies, and $V_{\rm disk}(r)$ and $V_{\rm circ}(r)$ are the circular velocities of the disk (cold gas plus stars) and the composite disk-bulge-halo system, respectively.

The formation of bulges out of unstable disk material is a complicated process. It is likely to involve bars, which are efficient in transporting gas inwards, and which subsequently dissolve to form the bulge. However, the details of the mass flow, and the shape parameters of the resulting bulge component are poorly understood, and we are forced to make some ad hoc assumptions. If the disk is unstable according to (25), we transform cold gas mass from the inside out to the bulge, whereby we assume that the inflow is such that it does not create a positive gradient in the surface density of the cold gas. This particular choice for extracting bulge material from the disk is based on extensive tests, and is optimized to yield stellar disks that are close to exponential. We shortly address the influence of these assumptions in Section 3.4.

At each time step we use an iterative procedure to compute the gas mass transformed to the bulge, $\Delta M_{\rm bulge}$, such that the resulting disk has $\alpha_{\rm max} = \alpha_{\rm crit}$. This mass $\Delta M_{\rm bulge}$ is assumed to form stars instantaneously with 100 percent efficiency, and the SN energy released by this burst of star formation is added to the energy released by the quiescent star formation in the disk at the disk radii from which the bulge material originates. This latter assumption has no important consequences for our results. If, for instance, we were to deposit all SN energy related with the bulge formation at $r = 0$, this does not alter any of our conclusions.

We model the bulge as a sphere with a Hernquist density profile:

$$\rho_b(r) = \frac{M_b}{2\pi} \frac{r_b}{r\,(r + r_b)^3}, \tag{26}$$

where r_b is a scale length (Hernquist 1990). Given our poor understanding of the detailed processes involved we use empirical relations to compute r_b. Andredakis, Peletier & Balcells (1995) have shown that the effective radius r_e (defined as the radius encircling half of the projected light) is directly related to the total B-band luminosity of the bulge by the empirical relation

$$M_B = -19.75 - 2.8 \log(r_e). \tag{27}$$

We use this relation to compute the scale length of the bulge, taking account of the fact that for a Hernquist sphere $r_e = 1.8153\, r_b$ (Hernquist 1990). In practice, our results do not depend on this simple scaling assumption. The main parameter for the bulge is its total mass; changes in its actual density distribution are only a second-order effect, and do not influence our results.

2.7 Stellar population modeling & chemical evolution

In order to convert the stellar masses into luminosities we use the latest version of the Bruzual & Charlot (1993) stellar population synthesis models. These models provide the luminosities $l_i(t, Z)$ of a single burst stellar population with a total mass of 1 $\mathrm{M}_\odot$ as function of age t and metallicity Z in various optical passbands i. In each disk annulus we keep track of the amount of stars formed at each time step, $\Delta M_*(t_k)$, as well as the metallicity of the cold gas $Z(t_k)$. This allows us to compute the total luminosity in that annulus, at any time step t_j, as

$$L_i(t_j) = \sum_{k=1}^{j} l_i[t_j - t_k, Z(t_k)]\, \Delta M_*(t_k). \tag{28}$$

In order to model the chemical enrichment of the ISM we follow the standard instantaneous recycling approximation (IRA). We assume that a fraction $\mathcal{R}$ of the mass in stars formed is instantaneously returned to the cold gas phase with a yield y (which is defined as the fraction of mass converted into stars that is returned to the ISM in the form of newly produced metals). In each disk annulus, and at each time step, mass conservation implies

$$\Delta M_{\rm cold} = \Delta M_{\rm cool} - (1 - \mathcal{R})\Delta M_* - \Delta M_{\rm eject} \tag{29}$$

and for the mass in metals one thus obtains

$$\begin{aligned} \Delta M_{\rm metal} \; &= \; Z_{\rm hot}\Delta M_{\rm cool} - Z_{\rm cold}\Delta M_{\rm eject} - \\ & \quad Z_{\rm cold}(1 - \mathcal{R})\Delta M_* + y\Delta M_* \end{aligned} \tag{30}$$

We use these two equations to track the evolution of the metallicity of the cold gas in the disk, $Z_{\rm cold}$, as function of both time and radius. Note that the mass that is ejected is forever lost from the galaxy. The associated metals are not used to enrich the hot gas in the halo, and $Z_{\rm hot}$ is therefore constant with time.

2.8 Detailed description of model parameters

We distinguish two different sets of parameters. The first set, which we call the *galaxy parameters*, consists of $M_{\rm vir}(0)$, λ, and a, and specify a particular model galaxy. The second set, the *model parameters*, consists of parameters that specify the particular formation model. The model parameters are as follows:

- Cosmology: Ω_0, Ω_Λ, $\Omega_{\rm bar}$, h, σ_8. In this paper we restrict ourselves to the currently popular ΛCDM cosmology with $\Omega_0 = 0.3$, $\Omega_\Lambda = 0.7$, $h = 0.7$, and $\sigma_8 = 1.0$. These parameters are currently favored by a large body of observations. For the baryon density we adopt $\Omega_{\rm bar} = 0.019\, h^{-2}$ as suggested by the observations of primordial deuterium abundances by Tytler et al. (1999).
- Halo structure: C_0, f, and γ. For our ΛCDM cosmology, Bullock et al. (2001) found that dark matter haloes in N-body simulations have $\gamma = 1.0$, $C_0 = 4.0$ and $f = 0.01$. Unless stated otherwise, we shall adopt these values.
- Star formation: $\varepsilon_{\rm SF}$, n, Q, and $\sigma_{\rm gas}$. For a large sample of disk galaxies and circum-nuclear starburst regions Kennicutt (1998) found $\varepsilon_{\rm SF} = 2.5 \times 10^{-4}\ \mathrm{M}_\odot \mathrm{yr}^{-1} \mathrm{kpc}^{-2}$ and $n = 1.4$, while it was shown in Kennicutt (1989) that for $\sigma_{\rm gas} = 6\ \mathrm{km\,s}^{-1}$ and $Q = 1.5$ the star formation truncation radii are in good agreement with observations. Since our star formation recipe is based on empirical relations, we keep our star formation parameters fixed at these observationally determined values.
- Feedback: $\varepsilon_{\rm fb}$. Since there are no empirical constraints on this feedback efficiency parameter we consider $\varepsilon_{\rm fb}$ a free parameter.
- Bulge formation: $\alpha_{\rm crit}$. This parameter sets the amount of self-gravity of the disk above which we transfer cold gas from the disk to the bulge. Numerical simulations by Christodoulou et al. (1995) found $\alpha_{\rm crit} = 0.7$ for a gaseous disk, which is what we adopt throughout.
- Stellar populations and chemical enrichment: $\eta_{\rm SN}$, $\mathcal{R}$, y, $Z_{\rm hot}$, and the choice for an initial mass function (IMF). Throughout we adopt the Scalo (1986) IMF, for which $\eta_{\rm SN} = 4 \times 10^{-3}\ \mathrm{M}_\odot{}^{-1}$ and $\mathcal{R} = 0.25$. We keep the stellar yield fixed at $y = 0.02$, which is a typical value used in chemical evolution models. Unless stated otherwise we adopt $Z_{\rm hot} = 0.3 Z_\odot$, typical of the hot gas in clusters (Mushotzsky & Loewenstein 1997).

3 THE DENSITY DISTRIBUTION OF DISK GALAXIES

3.1 Cooling properties

We start our investigation into the structural properties of our model galaxies by computing the density distributions of the cold gas disks in the absence of star formation, feedback, and bulge formation. To that extent we first examine the disk mass fractions as function of the various input parameters.

The free-fall time at each redshift z is the same for all galaxies as it depends only on the average halo density $\bar{\rho}(z) = \Delta_{\rm vir}(z)\, \rho_{\rm crit}(z)$. It increases from 0.08 Gyr at $z = 10$ to 2.2 Gyr at $z = 0$. The cooling time, on the other hand, depends on the density and (virial) temperature of

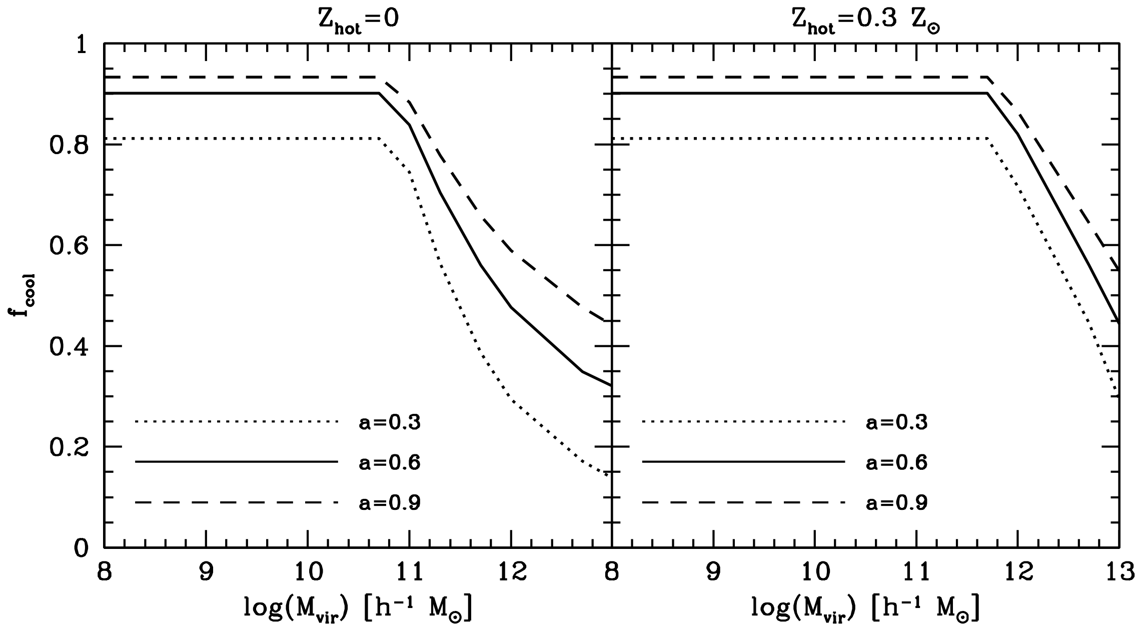

Figure 2. The fraction, $f_{\rm cool}$, of baryonic mass inside the virial radius that has cooled and settled in present day disks as function of the present day virial mass. Results are shown for three different MAHs, and for two different metallicities of the gas. For low mass systems $f_{\rm cool}$ depends only on the free-fall time and is independent of halo mass. For more massive systems $f_{\rm cool}$ is dominated by the cooling time scale and $f_{\rm cool}$ decreases rapidly with increasing mass. Accreting more mass at earlier times (i.e., larger a) and increasing the metallicity of the gas both result in larger values of $f_{\rm cool}$.

the gas, and is a strong function of $M_{\rm vir}$. In Figure 2 we plot the fraction $f_{\rm cool}$ of baryons inside the virial radius that has settled in the disk at $z = 0$ as function of the present day virial mass. Results are shown for three different values of a and for both zero-metallicity gas (left panel) and gas with a metallicity one-third Solar (right panel). For gas with $Z_{\rm hot} = 0$ and $M_{\rm vir}(0) \lesssim 10^{11} h^{-1} {\rm M}_{\odot}$ one finds that $t_{\rm cool} < t_{\rm ff}$ at all redshifts, and between 81 and 93 percent of the gas has settled in a disk by $z = 0$, depending on the MAH. For more massive systems the cooling time exceeds the free-fall time during the later stages of evolution, and less mass can cool. Consequently, $f_{\rm cool}$ decreases strongly with mass: for a system with $M_{\rm vir}(0) = 10^{13} h^{-1}\,{\rm M}_{\odot}$ only between 14 and 44 percent of the baryons inside the virial radius can cool. If the gas is pre-enriched to $Z_{\rm hot} = 0.3 Z_{\odot}$, the cooling is more efficient, and $f_{\rm cool}$ is significantly larger for high mass systems. To summarize, $f_{\rm cool}$ is a strong function of mass, MAH and metallicity, and one thus expects strong variations of the mass fractions of cold gas and stars in galaxies.

3.2 The density distribution of the gas

In Figure 3 we plot the surface density of the cooled gas and the total circular velocity at $z = 0$ as function of radius (no star formation or bulge formation is included here). The different panels show the results of varying one parameter with respect to a fiducial model with $M_{\rm vir}(0) = 5 \times 10^{11} h^{-1}\,{\rm M}_{\odot}$, $\lambda = 0.06$, $a = 0.6$, and $\gamma = 1.0$ (this model is plotted as a solid line in all panels). In the panels on the left we vary the spin parameter λ. As expected, systems with more angular momentum (larger λ) result in more extended disks. For $\lambda \lesssim 0.05$ the compact disks that form are strongly self-gravitating, resulting in strongly declining rotation curves. Once bulge formation is included, these systems will transform significant fractions of their disk mass in a bulge component, such that the final rotation curves are in agreement with observations (see Section 3.4). The middle panels of Figure 3 plot the results for three different MAHs. An earlier MAH (larger a) yields disks that are more centrally concentrated, but also more extended. This owes to the differences in the cooling histories of the gas. Galaxies with an earlier MAH have more gas cooled at high redshifts when the halo is denser. Consequently, that gas reaches centrifugal equilibrium at smaller radii. In addition, the final value of $f_{\rm cool}$ is higher (cf. Figure 2), and this excess gas cools to large radii, resulting in a more extended disk. Finally, in the panels on the right we plot results for three different values of γ. Less strongly cusped haloes (lower γ) result in more extended disks and lower values of $V_{\rm circ}$. This owes to the fact that haloes with lower γ are less dense, such that the gas reaches centrifugal equilibrium at larger radii.

As is immediately apparent from Figure 3, none of the disk surface density profiles resemble an exponential. In all cases the gas is much more centrally concentrated, and is well-fitted by a power-law $\Sigma_{\rm gas}(R) \propto R^{-n}$ with $1 \lesssim n \lesssim 2$. This confirms previous results by Kauffmann (1996), Dalcanton et al. (1997) and Firmani & Avila-Reese (2000), and is a direct consequence of the detailed conservation of angular momentum, and the fact that the dark matter haloes have (broken) power-law density distributions (see discussions in Seiden, Schulman & Elmegreen 1984 and Yoshii & Sommer-Larsen 1989). In order to produce stellar disks with an exponential surface density distribution out of these power-law gas disks one needs to either (i) have specifically tuned star formation efficiencies, (ii) transform part of the central gas disk into a bulge component, or (iii) somehow

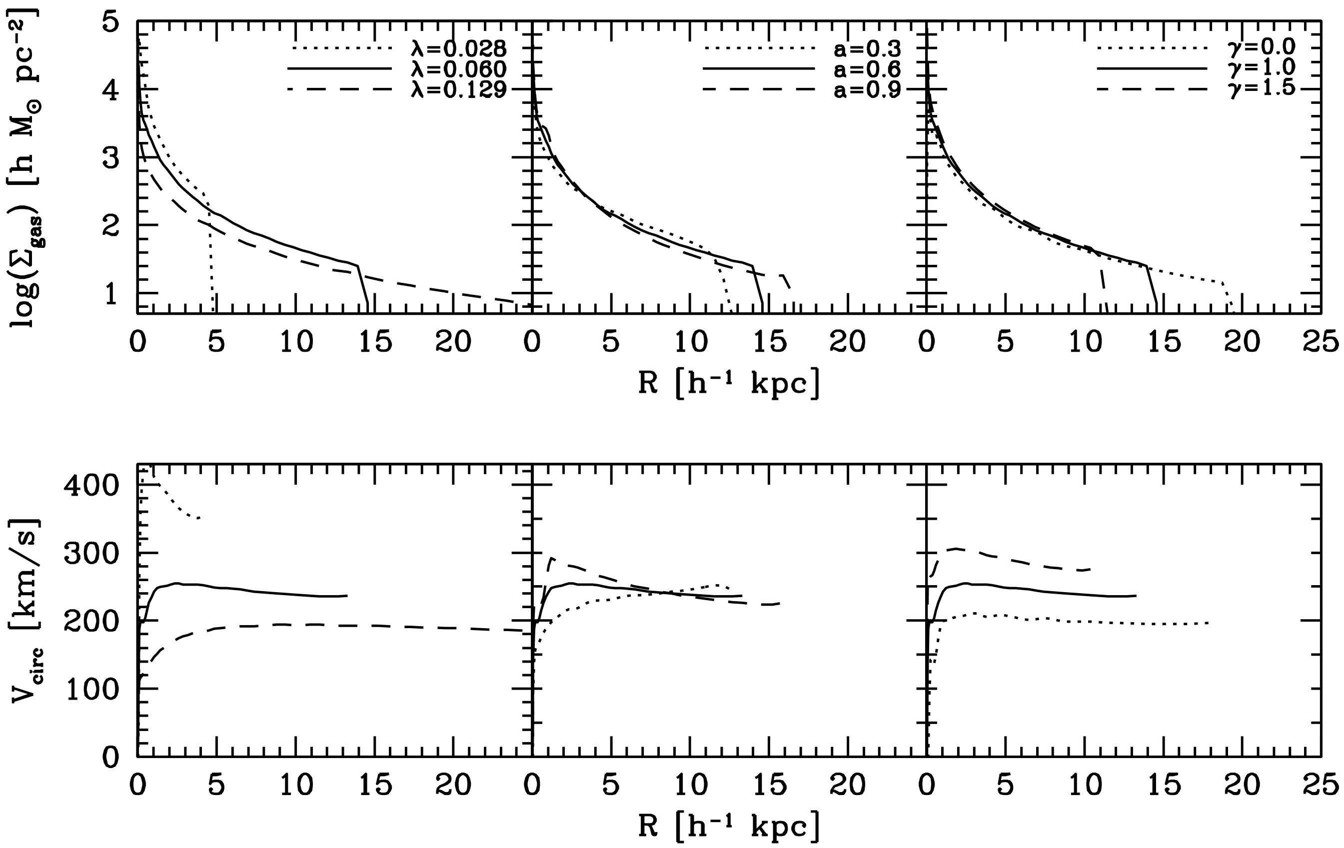

Figure 3. The upper panels plot the surface density distribution of cold gas as function of radius for models without star formation and bulge formation. The lower panels plot the corresponding circular velocity curves, out to the cut-off radius of the disk. All models have the same virial mass of $M_{\rm vir}(0) = 5 \times 10^{11} h^{-1}\ {\rm M}_{\odot}$. The solid lines correspond to the model with $\lambda = 0.06$ (median spin parameter), $a = 0.6$ ('average MAH') and $\gamma = 1.0$ (NFW halo profile). The dashed and dotted lines show the influence of varying one parameter as indicated in the top panels (see text for a discussion).

remove the central excess of gas from the disk. Below we examine how our particular recipes for star formation, bulge formation, and feedback fair in this respect.

3.3 The influence of star formation

We now include star formation in our models using the empirical parameters listed in Section 2.8. In Figure 4 we plot the present day surface densities of both the gas and stars as functions of the normalized radius $R/R_{\rm vir}$. Results are shown for six model galaxies that only differ in total mass and angular momentum as indicated in the various panels.

Except for the case with $M_{\rm vir}(0) = 5 \times 10^{9} h^{-1}\ {\rm M}_{\odot}$ and $\lambda = 0.129$ (lower right corner) all stellar disks are more concentrated than an exponential. Although the density distributions are reasonably close to exponential over their intermediate radial range, they harbor a pronounced central cusp and a distinct cut-off radius. The surface density of the cold gas follows $\Sigma_{\rm crit}$ (indicated by the thin dotted lines), except in the outer regions of the disk, where the gas has only recently been accreted, and star formation has not had sufficient time to deplete the density of the gas to $\Sigma_{\rm crit}$.

A comparison between the upper and lower panels of Figure 4 reveals that the lower mass systems produce disks of lower surface brightness and with higher gas mass fractions. As pointed out by previous studies, this scaling is in good agreement with observations (e.g., Dalcanton et al. 1997; Mo et al. 1998; van den Bosch 2000; van den Bosch & Dalcanton 2000). From Figure 4 it is also apparent that lower mass systems have larger ratios between the sizes of the gas disk and the stellar disk. We return to this issue in Section 4.

3.4 The influence of bulge formation

As already eluded to by Bullock et al. (2000), if the excess gas mass in the centres of the disks is transformed into a bulge component, this may solve the problem with the overly concentrated disks. We now examine whether the inclusion of our particular model for bulge formation, based on the idea that self-gravitating disks transform part of their material into a bulge, yields exponential stellar disks.

In Figure 5 we plot the $z = 0$ surface densities of the same models as in Figure 4, except that we now have included bulge formation (using the parameters listed in Section 2.8). The low angular momentum systems with $\lambda = 0.028$ have formed massive bulges with $M_{\rm bulge}/M_{\rm disk} = 0.7 - 0.8$ (i.e., they are more reminiscent of S0s than spiral galaxies). The bulge formation has depleted the cold gas in the centre to below $\Sigma_{\rm crit}$, suppressing subsequent star formation and resulting in a stellar disk that is remarkably exponential. The same applies to the systems with $\lambda = 0.06$ (middle panels), for which $M_{\rm bulge}/M_{\rm disk} \sim 0.07$, typical of

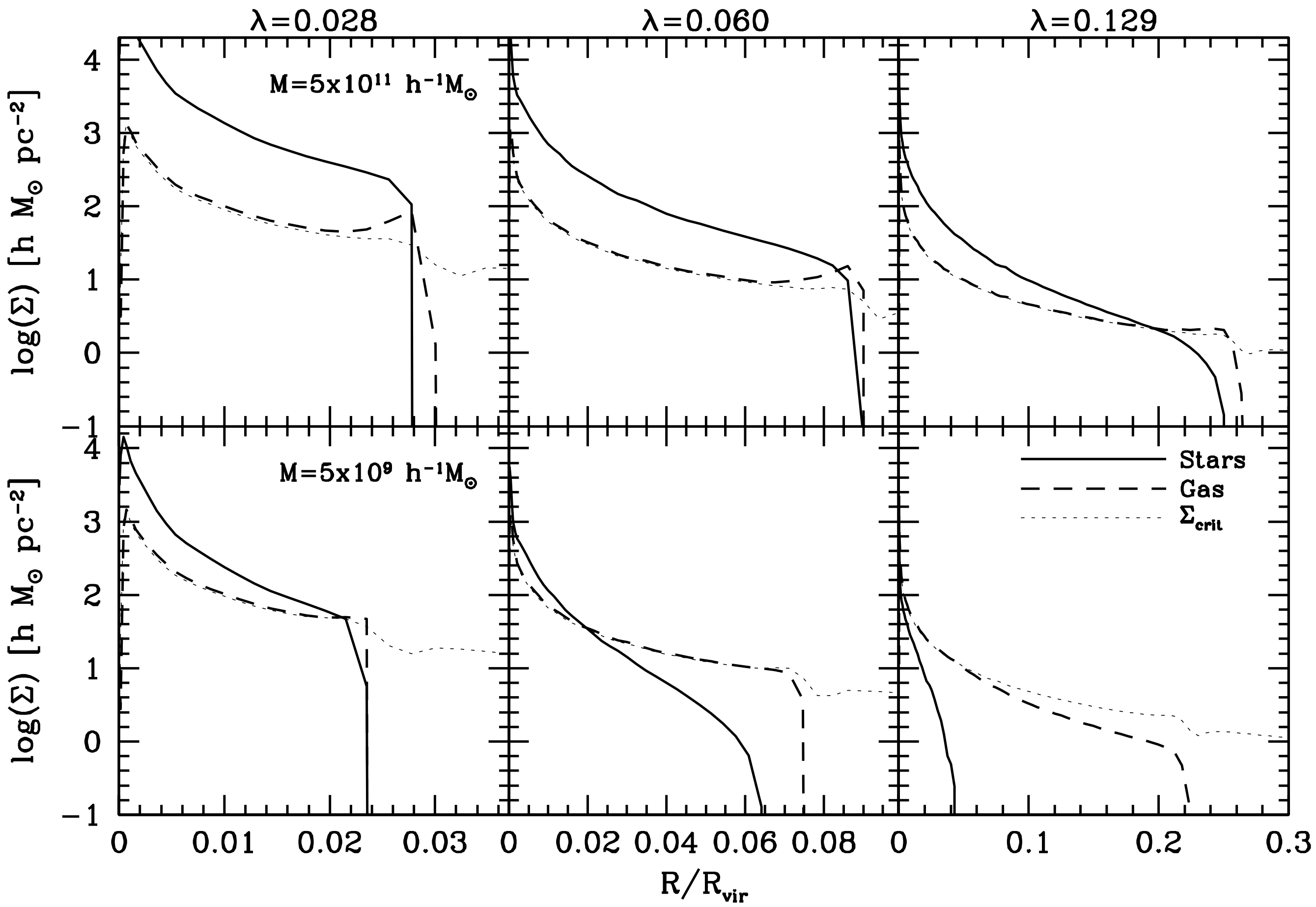

Figure 4. The $z = 0$ surface density profiles of the stars (solid lines) and cold gas (dashed lines) as functions of the normalized radius $R/R_{\rm vir}$. In addition, the critical surface densities for star formation are plotted as thin dotted lines. No bulge formation is taken into account here. The six models shown have the same MAH (with $a = 0.6$), but differ in total mass and angular momentum as indicated. Except for the model with $M_{\rm vir}(0) = 5 \times 10^9 h^{-1}\,{\rm M}_\odot$ and $\lambda = 0.129$, all stellar disks are more centrally concentrated than an exponential. See the text for a more detailed discussion.

late-type Sc spirals. Clearly, the formation of a bulge component out of the low angular momentum disk material seems fairly successful in producing exponential stellar disks. In the case with $\lambda = 0.129$, however, hardly any bulge component is produced ($M_{\rm bulge}/M_{\rm disk} = 0.001$). Consequently, the more massive models produce, as in the case without bulge formation, stellar disks with a central cusp in excess to the outer exponential profile. Depending on the radial range in which the exponential is fit, the cusp contains on the order of 20 to 30 percent of the mass of the stellar disk.

Recall that we model the inflow of the gas out of which the bulge is formed such that no positive gradient is created in the surface density of the cold gas (Section 2.6). This is a fairly ad hoc assumption, especially since it is well known that the actual HI distribution of disk galaxies often reveal a strong positive gradient reflecting a central hole in the HI distribution†. However, it turns out that the density distributions of the stellar disks are fairly insensitive to the details of the inflow-model. If, for instance, we model the gas inflow such that *all* the gas in the central bin is transformed into a bulge component before gas at larger radii is used (i.e., we resort to a maximally efficient inflow), the bulge dominated model galaxies reveal gas disks with large central holes, whereas the stellar disks are only marginally different from the standard inflow model. Thus, whereas our modeling of the bulge formation is admittedly crude, the main point is that despite the fact that we have optimized the cooling flow to produce exponential disks in systems with relatively large bulges, we are still left with the problem that the high angular momentum, low surface brightness systems, without a significant bulge component, have stellar disks that are more centrally concentrated than an exponential.

† It is currently still unclear to what extent these holes are truly devoid of gas, or whether they are actually filled with molecular or ionized gas.

3.5 The influence of feedback

The energy input into the ISM by supernovae can produce galactic winds that can drive mass out of the disk. Feedback is therefore a natural process that can reshape the density distributions of the disks. In order to solve the problem with the excess central densities we need the feedback process to be relatively more efficient in the centre than in the outer

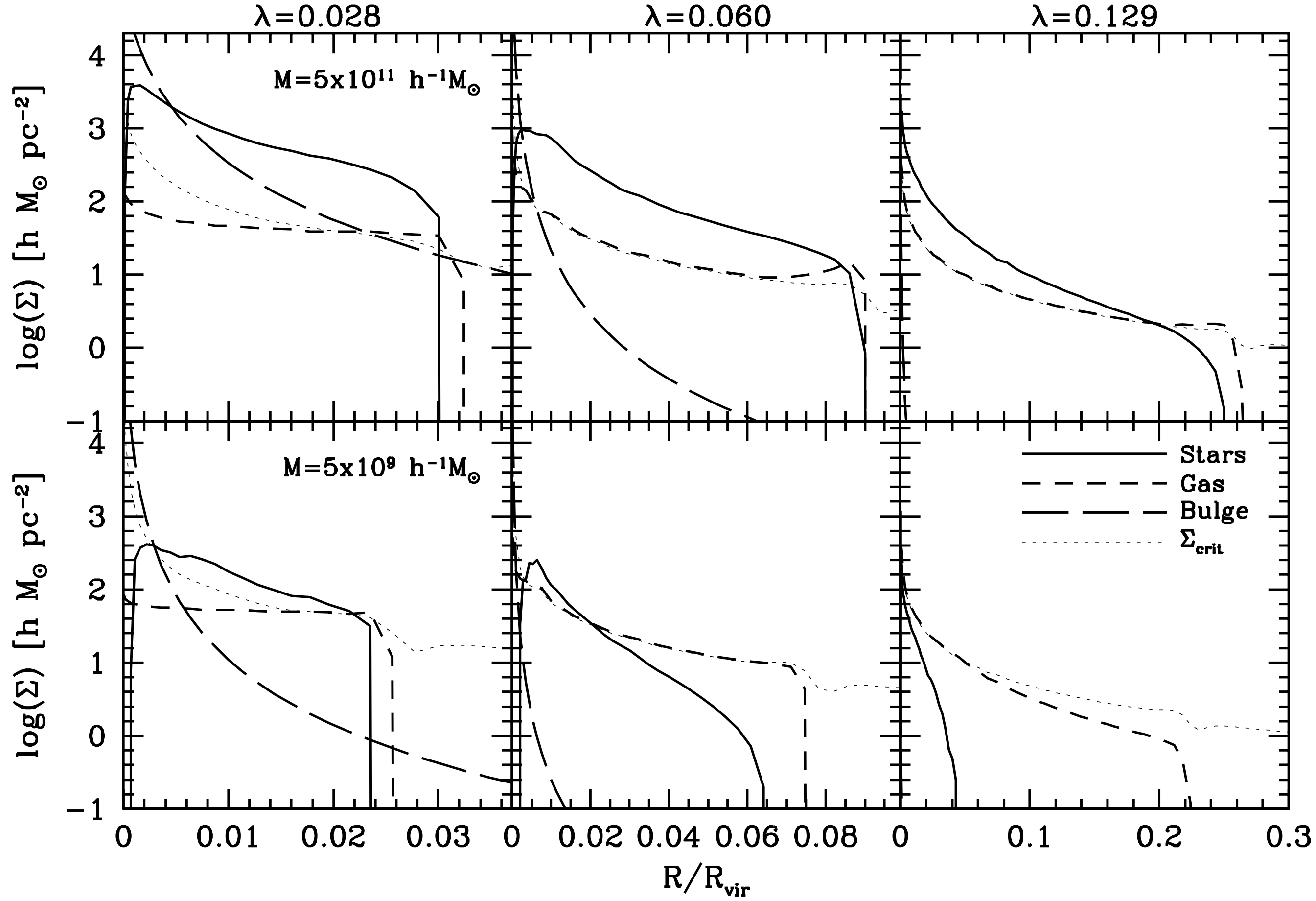

Figure 5. Same as Figure 4, except that now we have included bulge formation. In the cases with $\lambda = 0.028$ and $\lambda = 0.06$ significant bulges have formed out of the low angular momentum disk material, and the resulting stellar disks have surface density profiles that are close to exponential over their entire radial range. Systems with high angular momentum, however, do not produce a significant bulge component, and the stellar disks that form are similar to the case without bulge formation (cf. Figure 4).

parts of the disks. There are three effects that determine these relative efficiencies within our simple feedback picture: At smaller radii more stars form, and thus more SN energy is available to drive an outflow. At the same time, the escape velocities are higher at smaller radii, suppressing the efficiency of outflow. Finally, star formation at smaller radii starts earlier, when the total escape velocity of the system is still low. We now examine how these effects compete and whether or not we can produce bulge-less disks with exponential surface densities.

In Figure 6 we plot, for three different feedback efficiencies, the baryonic mass fractions at $z = 0$ in each radial bin that have ended up as bulge mass, disk stars, cold gas, or have been ejected. In the case without feedback (upper panel), virtually all the gas in the centre of the galaxy ends up in the bulge, while at larger radii, most of the gas is converted into disk stars. The introduction of a modest amount of feedback with $\varepsilon_{\rm fb} = 0.02$ (middle panel) suppresses both the bulge formation and the formation of disk stars. Most remarkably, the fraction of the gas mass that is ejected is almost constant with radius. Apparently the three effects mentioned above cancel each other out such that the fractional feedback efficiency is virtually independent of radius. In the case with $\varepsilon_{\rm fb} = 0.2$ (lower panel) the relative feedback efficiency is slightly higher in the centre than at larger radii, but the effect is not enough to alleviate the problem with the central cusps. We thus conclude that our simple picture of supernovae induced feedback does not significantly alter the density distribution of the resulting disk galaxies (except for an absolute offset), and thus can not solve the problem of the overly concentrated disks.

4 TRUNCATION RADII

As is evident from Figure 5, our models reveal distinct truncation radii in the density distributions of both the stars and the gas. The truncation radius of the cold gas reflects the maximum specific angular momentum of the baryonic mass that has cooled. The truncation radius of the stars, on the other hand, reflects the presence of a star formation threshold density.

In order to make a quantitative comparison with the observed truncation radii in disk galaxies, we construct three samples of 100 model galaxies. The samples only differ in the value of the feedback efficiency; all other model parameters are kept fixed at their fiducial values listed in Section 2.8. Masses are drawn randomly from a uniform distri-

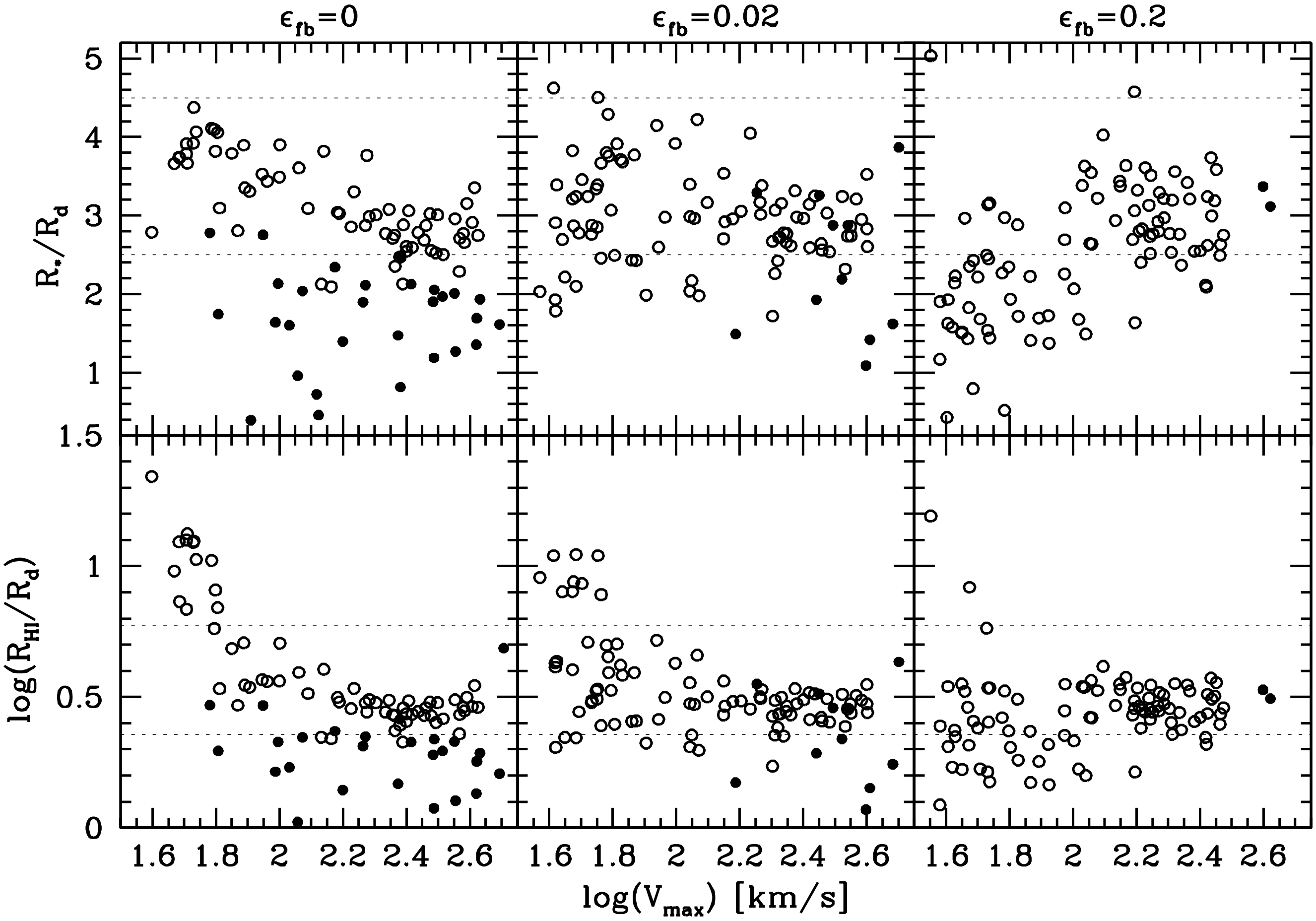

Figure 7. The ratios R_*/R_d (upper panels) and $R_{\rm HI}/R_d$ (lower panels) as functions of $\log(V_{\rm max})$. Results are plotted for three samples of 100 model galaxies each, that only differ in the value of the feedback efficiency as indicated above each column. Open (filled) circles correspond to models with bulge-to-disk mass ratio less (more) than 0.2. The horizontal dotted lines indicate the range of observed values: $R_*/R_d = 3.5 \pm 1.0$ and $R_{\rm HI}/R_d = 4.1 \pm 1.8$. See text for a detailed discussion.

bution with $3 \times 10^9 h^{-1}\,{\rm M}_{\odot} \leq M_{\rm vir}(0) \leq 3 \times 10^{12} h^{-1}\,{\rm M}_{\odot}$, the spin parameter is drawn from the probability distribution of equation (11) with $\bar{\lambda} = 0.06$ and $\sigma_{\lambda} = 0.6$, and the MAH parameter a is drawn from a Gaussian distribution with $\bar{a} = 0.6$ and $\sigma_a = 0.15$. For each model galaxy we determine the radii R_*, $R_{\rm gas}$, and $R_{\rm HI}$. Here we define R_* as the maximum radius with non-zero surface density of stars, $R_{\rm gas}$ as the maximum radius with non-zero surface density of cold gas, and $R_{\rm HI}$ as the radius at which the surface density of the cold gas is equal to $1.3\,{\rm M}_{\odot}{\rm pc}^{-2}$. Taking account of the Helium mass abundance, $R_{\rm HI}$ thus corresponds to the radius where the HI surface density is equal to $1.0\,{\rm M}_{\odot}{\rm pc}^{-2}$. In order to express these truncation radii in terms of the scale length of the stellar disk we fit an exponential to the I-band surface brightness profiles of the models. Since, as we have shown above, not all stellar disks are well-fit by an exponential, there is some ambiguity involved in these fits. After some experimenting we found adequate results upon restricting the fits to the radial interval $0.2R_* \leq R \leq 0.9R_*$, which is what we adopt throughout.

4.1 The extent of stellar disks

The upper panels of Figures 7 and 8 plot R_*/R_d as function of the maximum of the rotation curve and the central I-band surface brightness of the best-fit exponential, respectively. Observations have shown that stellar disks in spiral galaxies reveal truncation radii, R_*, in the range from 2.5 to 4.5 disk scale lengths (van der Kruit & Searle 1981a,b; Romanishin, Strom & Strom 1983; Barteldrees & Dettmar 1994; Pohlen, Dettmar & Lütticke 2000; de Grijs, Kregel & Wesson 2001). This range is indicated by horizontal dotted lines. It is important to realize that most studies of stellar truncation radii have focussed on disk galaxies with small bulges. Therefore, in order to make a fair comparison with our models, we plot model galaxies with $M_{\rm bulge}/M_{\rm disk} > 0.2$ with separate symbols (filled circles).

In the case without feedback (left panels) the model galaxies with $M_{\rm bulge}/M_{\rm disk} \leq 0.2$ (open circles) have stellar cut-off radii $2 \lesssim R_*/R_d \lesssim 4.5$, in excellent agreement with observations. In addition, the models predict that the more bulge-dominated galaxies have $R_*/R_d \lesssim 2$. It should be relatively straightforward to test this prediction with deep photometry of a sample of Sa and S0 galaxies.

Increasing the feedback efficiency reduces the average

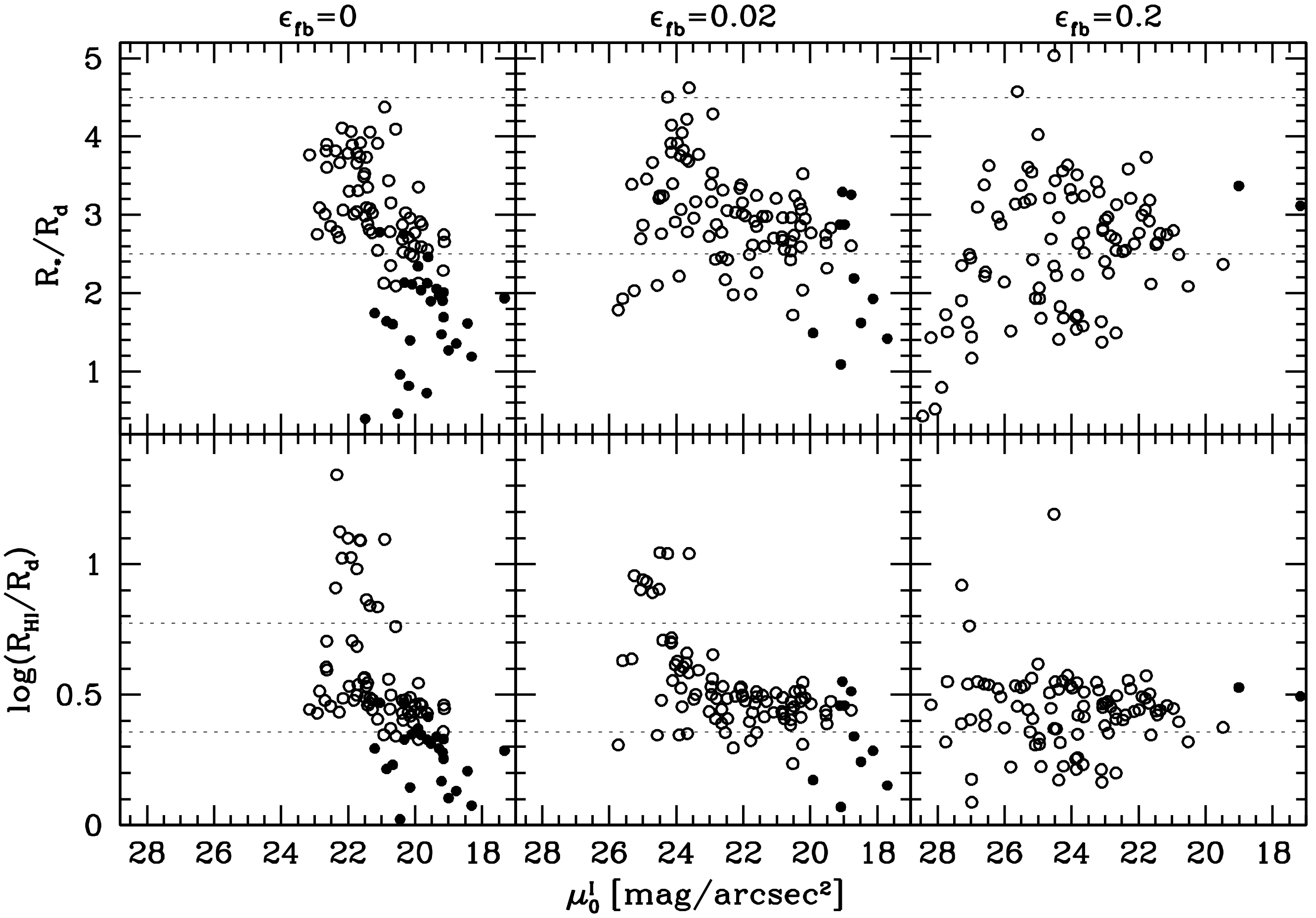

Figure 8. Same as Figure 7 except that now R_*/R_d and $R_{\rm HI}/R_d$ are plotted as functions of the I band central surface brightness of the best fit exponential.

bulge-to-disk ratio of the models and produces disks with lower central surface brightnesses. In the case where $\varepsilon_{\rm fb} = 0.2$ only two of the model galaxies have $M_{\rm bulge}/M_{\rm disk} > 0.2$. Furthermore, the models now predict that low-mass systems should have values of $R_*/R_d \lesssim 2.5$, significantly lower than for the more massive systems. Unfortunately most studies of stellar truncation radii have focussed on more massive disk galaxies, and a more detailed comparison of our models with observations has to await more data, especially on dwarf and LSB galaxies. Nevertheless, it is reassuring that our models with $M_{\rm bulge}/M_{\rm disk} \lesssim 0.2$ have stellar truncation radii in good agreement with observations, supporting the idea that they originate from a star formation threshold density set by Toomre's stability criterion.

4.2 The extent of gas disks

Little is known about the truncation radii of the gaseous component of disk galaxies, mainly due to the fact that the gas is generally probed by the HI. Since at column densities below $\sim 10^{19}\,{\rm cm}^{-2}$ one expects the gas to be ionized by the cosmic background flux of ionizing photons (e.g., Sunyaev 1969; Maloney 1993), a truncation in the HI does not necessarily reflect the true outer edge of the gas disk. Therefore, one typically expresses the size of the gas disk by the radius $R_{\rm HI}$ at which the HI surface density is equal to $1.0\,{\rm M}_{\odot}{\rm pc}^{-2}$ ($1.2 \times 10^{20}\,{\rm cm}^{-2}$).

The lower panels of Figures 7 and 8 plot $R_{\rm HI}/R_d$ as function of $V_{\rm max}$ and μ_0^I, respectively. Systems with $M_{\rm bulge}/M_{\rm disk} > 0.2$ typically have $R_{\rm HI}/R_d \lesssim 3$. For the galaxies with lower bulge-to-disk ratios we find that $R_{\rm HI}/R_d = 2.8 \pm 0.5$ for $V_{\rm max} > 150\,{\rm km\,s}^{-1}$ and $R_{\rm HI}/R_d \gtrsim 3$ for $V_{\rm max} < 150\,{\rm km\,s}^{-1}$. For a sample of 73 dwarf galaxies with $V_{\rm max} \lesssim 100\,{\rm km\,s}^{-1}$ Swaters (1999) found an average of $R_{\rm HI}/R_d = 4.1 \pm 1.8$ (with R_d measured in the R-band, which we assume to be roughly equal to that in the I-band). This is in good agreement with our models with $\epsilon_{\rm fb} = 0$ and $\epsilon_{\rm fb} = 0.02$. However, the model with $\epsilon_{\rm fb} = 0.2$ yields and average of $R_{\rm HI}/R_d = 2.3$ for galaxies with $V_{\rm max} < 100\,{\rm km\,s}^{-1}$, which is only marginally consistent with the data.

In Figure 9 we plot the ratio $R_{\rm gas}/R_{\rm HI}$ as function of μ_0^I for the model without feedback (left panel). Models with $\epsilon_{\rm fb} = 0.02$ and 0.2 yield very similar results. Except for low mass LSB galaxies with $\mu_0^I \gtrsim 22$ mag arcsec^{-2}, we find that $R_{\rm gas} \simeq R_{\rm HI}$, indicating that the physical truncation of the cold gas occurs close to the radius where $\Sigma_{\rm HI} = 1.0\,{\rm M}_{\odot}\,{\rm pc}^{-2}$. We can compare these model predictions to data by computing the ratio $R_{\rm HI,max}/R_{\rm HI}$, where $R_{\rm HI,max}$ is defined as the maximum radius out to which HI is detected. $R_{\rm HI,max}$ can thus be considered a *lower* limit on $R_{\rm gas}$. Results for

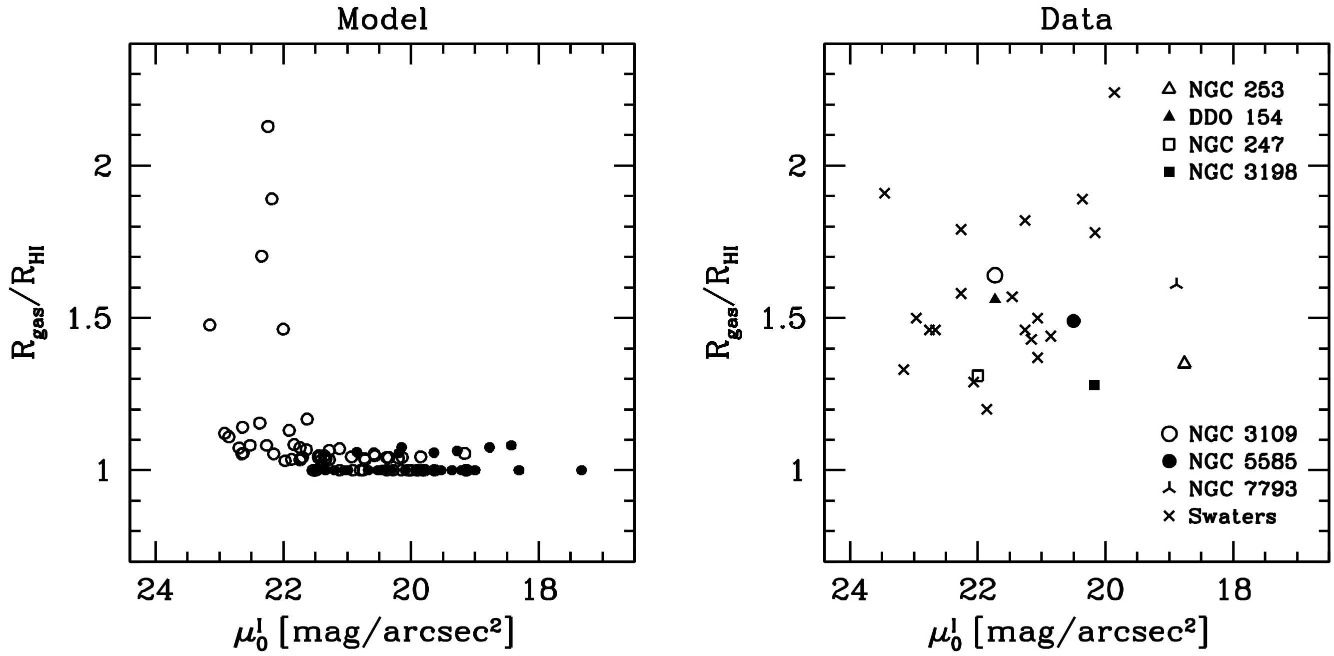

Figure 9. The ratio $R_{\rm gas}/R_{\rm HI}$, between the actual cut-off radius of the gas disk ($R_{\rm gas}$) and the radius where the HI surface density equals 1.0 $\rm M_\odot\ pc^{-2}$ ($R_{\rm HI}$), as function of the I-band central surface brightness. The panel on the left shows the results for a sample of 100 model galaxies with $\epsilon_{\rm fb} = 0.0$ (all other model parameters are set to their fiducial values, see Section 2.8). Symbols are as in Figures 7 and 8. Note how, except for a few low mass LSB galaxies, all models have $R_{\rm gas} \simeq R_{\rm HI}$; the truncation of the model gas disks occurs close to the radius where $\Sigma_{\rm HI} = 1.0\,\rm M_\odot\,pc^{-2}$. This is in clear conflict with the data for 26 disk galaxies with readily available HI surface brightness profiles, plotted in the right panel. Here $R_{\rm gas}$ is the maximum radius out to which HI (or Hα) is detected, and thus corresponds to a *lower* limit on the actual cut-off radius. Data is taken from the following sources: DDO 154 (Carignan & Beaulieu 1989), NGC 247 (Carignan & Puche 1990a), NGC 3198 (Begeman 1989), NGC 3109 (Jobin & Carignan 1990), NGC 5585 (Côté, Carignan & Sancisi (1991), NGC 7793 (Carignan & Puche 1990b), and Swaters (1999). If no I-band surface brightness data is available we used the colors of de Jong (1996) for conversion. NGC 253 is a special case. This galaxy in the Sculptor group is the only galaxy in which ionized gas has been detected at radii beyond $R_{\rm HI}$ (Bland-Hawthorn, Freeman & Quinn 1997). With $R_{\rm HI} = 8.6$ kpc (Puche, Carignan & van Gorkum 1991) and Hα and [NII] detected out to 11.6 kpc, this implies a lower limit of $R_{\rm gas}/R_{\rm HI} = 1.35$.

a number of disk galaxies with readily available HI surface brightness profiles are shown in the right panel of Figure 9. As is evident from Figure 9, real galaxies have HI disks that extend to at least $\sim 1.5 R_{\rm HI}$. At these radii the HI surface density typically has fallen to $\sim 0.1\ \rm M_\odot\ pc^{-1}$. Recall that these maximum radii are lower limits to the actual edge of the gas disk. Higher sensitivity HI and/or Hα observations are required to determine the true extent of the disks. For the moment, however, it is sufficient to realize that our models, which predict truncation radii close to where $\Sigma_{\rm HI} = 1.0\ \rm M_\odot\ pc^{-2}$, are in clear conflict with the data.

5 A NEW PROBLEM FOR THE FORMATION OF DISK GALAXIES

As shown above our models predict that LSB galaxies reveal surface brightness profiles that are more centrally concentrated than an exponential. The majority of observed LSB disk galaxies, however, have surface brightness profiles that are accurately fit by an exponential down to the very centre (McGaugh & Bothun 1994; de Blok, van der Hulst, & Bothun 1995; Swaters 1999). An exception are the giant, massive LSB disk galaxies, which have surface brightness profiles that are more concentrated than an exponential, but this reflects the presence of a relatively massive bulge component (Sprayberry et al. 1995; Pickering et al. 1997). Our failure to reproduce bulge-less LSB disks with exponential surface brightness profiles must thus be considered a failure of the models.

In addition, we have shown that whereas our implementation of star formation threshold densities yields stellar truncation radii in good agreement with observations, the models predict truncation radii in the gaseous component at too high surface density. Both of these problems indicate that our models predict disk galaxies that are too concentrated, and in what follows we shall refer to this as the *disk concentration problem* (hereafter DCP). Below we examine whether this DCP might be an artifact of the over-simplified nature of our models by discussing how various modifications of the ingredients or assumptions of our model influence the density distribution of the resulting disks.

5.1 Star formation, galactic winds, and AGNs

Although we adhere to empirical relations to model the star formation in the disk, one could easily envision an alternative model that results in relatively lower star formation efficiencies in the central regions. Although this might produce stellar disks that more closely resemble exponentials, it does not solve the problem at hand. Changing the star formation efficiencies only changes the relative ratio of gas to

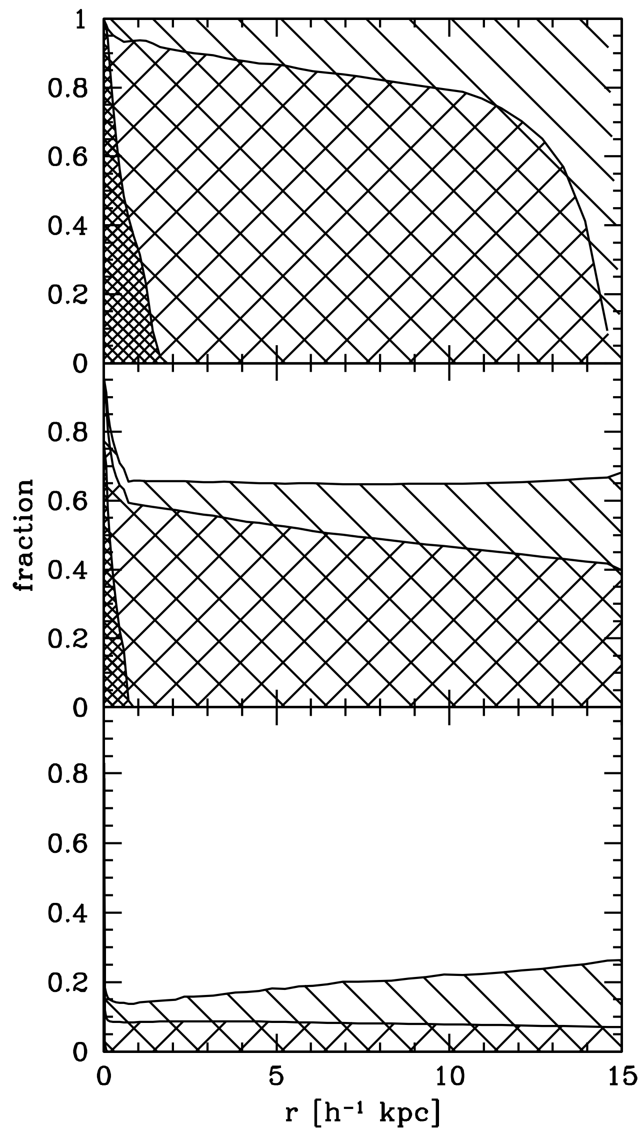

Figure 6. The fractions of the baryonic mass in each radial bin that, at $z = 0$, have ended up as bulge mass (densely cross-hatched regions), disk stars (loosely cross-hatched regions), cold gas (diagonally-hatched regions), or that have been ejected (white areas). All three panels correspond to the fiducial model galaxy with $M_{\rm vir}(0) = 5 \times 10^{11} h^{-1}\,{\rm M}_{\odot}$, $\lambda = 0.06$, $a = 0.6$, and $\gamma = 1.0$, but differ in the feedback efficiency: $\varepsilon_{\rm fb} = 0.0$ (upper panel), 0.02 (middle panel), and 0.2 (lower panel). Note how the baryonic mass fraction that is ejected depends only weakly on radius.

stars, while leaving the central *mass* densities intact. Therefore, such modifications will not alter the circular velocity curves, which, at least for the bulge-less LSB galaxies, seem inconsistent with observations (see Section 5.4 below).

A more plausible solution involves somehow removing the excess gas from the centres of the galaxies, or preventing it from reaching the centre in the first place. Feedback processes seem the most natural means to accomplish this. However, as shown in Section 3.5, our simplistic picture of SNe induced galactic winds is unable to solve the problem at hand. What is needed is a feedback process that is relatively more efficient at the centre than at larger radii. It is not inconceivable that a more sophisticated treatment of stellar feedback might actually accomplish that. For instance, the presence of active galactic nuclei (AGNs), which have been ignored in our models, might provide an additional amount of energy input exactly at the centre of the galaxies where it is most required. However, numerous studies have shown that the mass of the AGN's energy source, the massive black hole, is proportional to the mass of the bulge in which the AGN is embedded (Kormendy & Richstone 1995; Ferrarese & Merritt 2000; Gebhardt et al. 2000). Since the DCP is most severe for bulge-less systems, where one thus expects no (significant) AGN, it seems unlikely that the inclusion of AGN related feedback processes can solve the problem with the overly concentrated LSB galaxies. Nevertheless, because of our extremely limited understanding of the various feedback processes that are likely to play a role in the formation and evolution of (disk) galaxies, it is premature to exclude feedback as a mechanism that may solve the problem with the central concentration of the LSB model galaxies.. However, it is very unlikely that feedback processes can actually solve the problem with the truncation radii of the gas component, which manifests itself at radii beyond the stellar disk, and feedback as a solution to both aspects of the DCP thus seems unlikely.

5.2 Viscosity

We have not included viscous transport in our models. Viscosity is efficient in redistributing the disk's angular momentum distribution, and thus in modifying the density distribution of the disk material. Numerous studies in the past have in fact argued that, as long as the viscosity time scale is similar to the star formation time scale, viscous transport has the natural tendency to produce exponential disks, independent of the initial density distribution of the gas disk (Lin & Pringle 1987; Yoshii & Sommer-Larsen 1989; Clarke 1989; Olivier, Blumenthal & Primack 1991; Ferguson & Clarke 2001). However, there are two important caveats here. First of all, in most cases the resulting stellar disk has a density distribution that is only exponential in the outer regions, while the central regions reveal a central cusp, reminiscent of our disk profiles. Secondly, virtually all studies of viscous disks start with an initial density distribution that is less concentrated than an exponential. However, we have shown that the standard model for disk formation predicts density distributions that are already too concentrated, even before the onset of viscosity. Finally, it is worth stressing that the main mechanism for viscosity is poorly constrained, and in particular, that there is no detailed theory that links the time scale of viscosity to that of star formation, as required.

Most importantly, viscous transport is oriented inward in the central regions and outward in the outer regions. Thus, whereas viscosity seems the natural solution for the problem with the truncation radii, it will at the same time only aggravate the problem with the overly concentrated LSB galaxies. We thus do not consider viscosity a viable solution to the DCP.

5.3 The mass accretion histories of dark matter haloes

The DCP outlined above only applies to LSB galaxies. Throughout, it has been assumed that LSB galaxies only

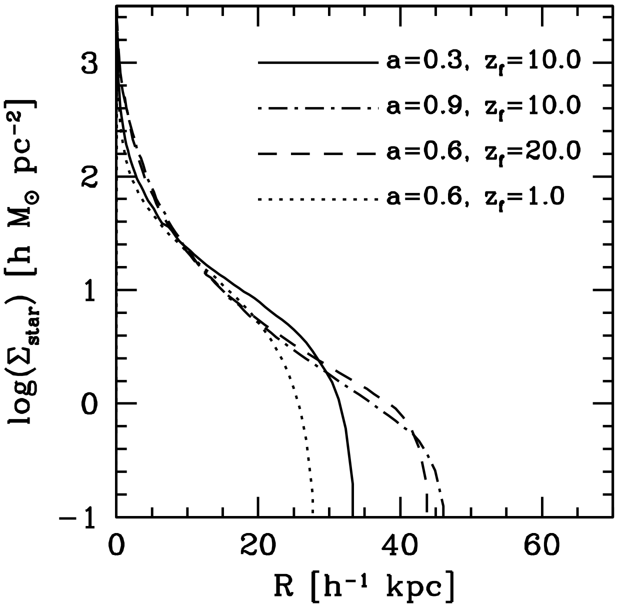

Figure 10. The influence of the MAH on the stellar surface density profiles of the disks. Plotted are $\log(\Sigma_{\rm star}(R))$ for four model galaxies with $M_{\rm vir}(0) = 5 \times 10^{11} h^{-1}$ M$_{\odot}$ and $\lambda = 0.129$. The models only differ in the values of z_f and a that parameterize the MAH. Note how despite a wide range in MAHs, the resulting disks all are too centrally concentrated to be consistent with observations. This illustrates that the DCP is not solved by resorting to specifically tuned mass accretion histories.

distinguish themselves from HSB galaxies in a larger spin parameter. Several studies have shown that this assumption is consistent with a wide variety of observed properties of LSB galaxies (e.g., Dalcanton et al. 1997; Mo et al. 1998; Jimenez et al. 1998). One important shortcoming of these models, however, is that they offer no explanation for the fact that LSB galaxies are less strongly clustered than their HSB counterparts (Mo, McGaugh & Bothun 1994). This has prompted several authors to suggest that differences in disk surface density are driven by differences in the amplitude of the original density fluctuations from which the galaxies arise (e.g., McGaugh & de Blok 1998). In this case, HSB and LSB galaxies are expected to have correlation functions with different amplitudes.

If indeed peak height is the main parameter that discriminates LSB from HSB galaxies one expects the two to have different MAHs (the amplitude of density perturbations is directly related to the halo formation epoch). It is therefore worthwhile to examine whether the disk concentration problem for LSB galaxies may be solved by resorting to different MAHs. Furthermore, as emphasized in Section 2.2, we have limited ourselves to a fairly small subset of possible MAHs by only considering models with $z_f = 10.0$ and a in the range $[0.3, 0.9]$. Clearly, a more extended exploration of parameter space is needed before we can actually claim a failure of the models to produce realistic LSB galaxies.

In Figure 10 we plot the stellar surface densities of four models with $M_{\rm vir}(0) = 5 \times 10^{11} h^{-1}$ M$_{\odot}$ and $\lambda = 0.128$ (all other parameters are set to the fiducial values listed in Section 2.8). The models only differ in their values of z_f and a as indicated. As is evident, the MAH mainly influences the extent of the disk that forms (due to its effect on the cooling history, see Section 3.1), but has a negligible effect on the central density of the disk. All four models, which have wildly different MAHs, yield disks that are inconsistent with the observed surface brightness profiles of LSB disk galaxies. In particular, the case with $z_f = 1.0$ (dotted line), which is the most appropriate for a scenario in which LSB galaxies form from low amplitude density fluctuations, yields a surface brightness profile that is only approximately exponential over a very small radial range. Clearly, the DCP can not be solved by resorting to specifically tuned MAHs. Note, however, that in principle haloes that form later will also be of lower density, something not taking into account in these models (see discussion in Section 2.2). We address this influence of halo density on the surface brightness profiles of the disks in the next section.

5.4 The nature of dark matter

In the standard picture for disk formation, outlined above, the density distribution of the disk is related to both the density and angular momentum distribution of the dark matter halo. If the dark matter is cold and collisionless it virializes to produce strongly concentrated haloes with steep central cusps. The disks that form in these haloes will therefore also be strongly concentrated. A possible solution to the DCP, therefore, might be that dark matter haloes are less concentrated, e.g., they have a constant density core. It is noteworthy in this context that numerous studies in recent years have claimed that the observed rotation curves of dwarf and LSB galaxies imply dark matter haloes with constant density cores (Flores & Primack 1994; Moore 1994; McGaugh & de Blok 1998, but see van den Bosch et al. 2000 and van den Bosch & Swaters 2001). Furthermore, if LSB galaxies form from low amplitude density fluctuation (see Section 5.3), one expects LSB galaxies to be embedded in low-density dark matter haloes Therefore, it is worthwhile to explore to what extent a modification of the dark matter density distribution can solve the DCP.

The two parameters in our models that set the dark matter density distributions are the central cusp slope γ and the normalization of the halo concentrations C_0. In the upper left panel of Figure 11 we plot the stellar surface densities of four models with $M_{\rm vir}(0) = 5 \times 10^{11} h^{-1}$ M$_{\odot}$, $\lambda = 0.128$ and $a = 0.6$. Our standard ΛCDM model with $\gamma = 1.0$ and $C_0 = 4.0$ (solid lines) yields a nearly bulge-free disk ($M_{\rm bulge}/M_{\rm disk} \simeq 0.001$) with a central cusp (cf. upper right panel of Figure 5). The disk is so strongly concentrated that the rotation curve (upper right panel) reveals a steep rise followed by a modest decline. This is another manifestation of the DCP, as the observed rotation curves of LSBs reveal a slow rise in the central parts and virtually never a declining part. The dot-dashed line shows the surface brightness profile for the same model galaxy but with $C_0 = 1.0$. This results in a halo concentration parameter c that is a factor four times smaller ($c = 3.7$ compared to $c = 14.8$). Eventhough the mass of the resulting galaxy is significantly less concentrated, as is evident from the rotation curves, the surface brightness of the resulting stellar disk is only marginally less concentrated. The main effect of reducing the halo concentration is to produce a more extended disk, and to increase the bulge-to-disk ratio (lower

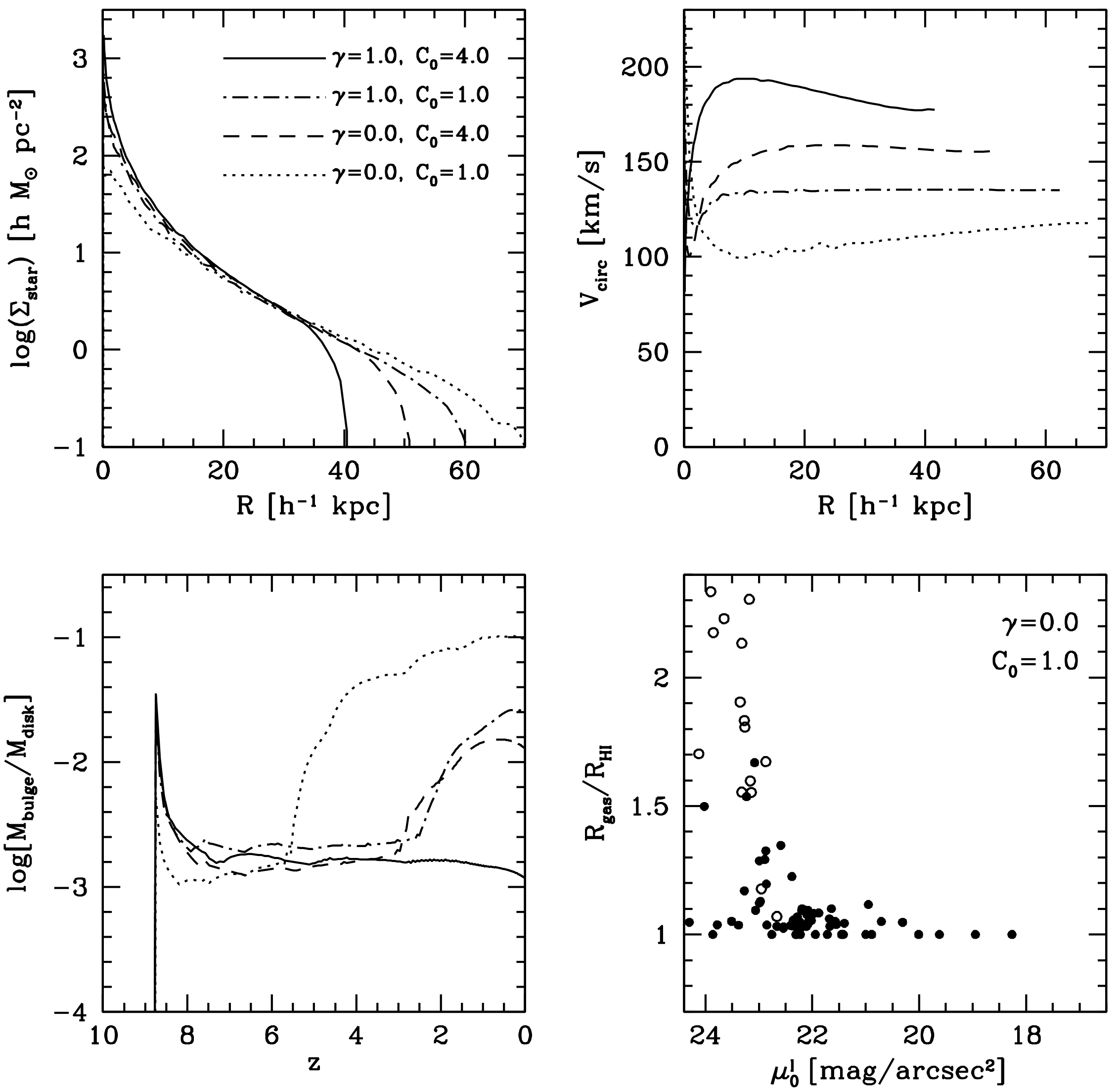

Figure 11. Properties of model galaxies with $M_{\rm vir}(0) = 5 \times 10^{11} h^{-1}$ M$_{\odot}$, $\lambda = 0.129$ and $a = 0.6$ for four different dark matter density distributions. The solid lines correspond to the standard ΛCDM haloes, with $\gamma = 1.0$ (i.e., haloes have NFW density profiles) and $C_0 = 4.0$. The dot-dashed lines correspond to a model with a halo concentration parameter that is four times smaller ($C_0 = 1.0$). Dashed lines correspond to a model with a constant density core ($\gamma = 0.0$), but with the same concentration parameter as our fiducial ΛCDM model. The dotted lines, finally, corresponds to a constant density cores with a core radius four times larger than for the standard model. The upper panels plot the surface densities of the stellar disks and the circular velocity curves (out to the truncation radius of the cold gas) as function of radius. The lower left panel plots the bulge-to-disk ratios (in mass) as function of redshift. Note how less concentrated dark matter haloes yield more extended disks with close-to-exponential density distributions and rotation curves that rise more slowly, in better agreement with observations. However, because the disks are more self-gravitating they also produce larger bulges, and the problem of producing bulge-less LSB disk galaxies with exponential stellar disks remains. Finally, the lower right panel plots the ratio $R_{\rm gas}/R_{\rm HI}$ as function of μ_0^I for 100 model galaxies with $\gamma = 0.0$ and $C_0 = 1.0$. Symbols are as in Figure 9. Note how even for dark matter haloes with large constant density cores the truncation radii of the gas disks in HSB systems occurs close to $R_{\rm HI}$, in conflict with observations.

left panel). Clearly, merely changing the halo concentrations is not able to solve the DCP.

The dashed lines in Figure 11 show the results for the same model galaxy but with $C_0 = 4.0$ and $\gamma = 0.0$, i.e., rather than changing the halo concentration parameter, we now consider dark matter haloes with a constant density core rather than a r^{-1} cusp. The results of lowering γ are fairly similar to those of lowering C_0: the resulting stellar disk is somewhat less concentrated and more extended than for the case with the NFW dark matter halo, but the stellar density distribution is still significantly more concentrated than a pure exponential. Furthermore, the bulge-to-disk ratio is an order of magnitude larger than in the standard case with $\gamma = 1.0$ and $C_0 = 4.0$.

The dotted lines, finally, correspond to a model with $\gamma = 0.0$ and $C_0 = 1.0$. In this case the stellar disk is close to exponential over a relatively large radial range, and the central cusp has largely disappeared. Furthermore, the resulting rotation curve is still rising at the outer edge of the gas disk, in better agreement with observations. However, as can be seen from the lower left panel, the bulge-to-disk ratio is, with $M_{\rm bulge}/M_{\rm disk} = 0.1$, two orders of magnitude larger than for the ΛCDM model with $\gamma = 1.0$ and $C_0 = 4.0$. This emphasizes the robustness of the DCP. When trying to lower the central densities of the disks by resorting to dark matter haloes of lower (central) densities, the disks become more self-gravitating, which results in larger disk-to-bulge ratios. The problem of producing bulge-less exponential stellar disks therefore remains

Finally, the lower right panel plots $R_{\rm gas}/R_{\rm HI}$ as function of μ_0^I for a sample of 100 model galaxies with $\gamma = 0.0$ and $C_0 = 1.0$. Compared to the ΛCDM model with $\gamma = 1.0$ and $C_0 = 4.0$ (left panel of Figure 9), both the fraction of low surface brightness galaxies and that of systems with $M_{\rm bulge}/M_{\rm disk} \geq 0.2$ have increased. However, systems with $\mu_0^I \lesssim 22$ mag arcsec^{-2} still have $R_{\rm gas}/R_{\rm HI} \simeq 1$, in disagreement with observations. Modifying the structure of the dark matter haloes can thus not solve the problem with the truncation radii outlined in Section 4.

5.5 The angular momentum

Under the assumption of angular momentum conservation, the density distribution of the disk that forms is a direct reflection of the angular momentum distribution of the baryons in the protogalaxy. The DCP might therefore be a consequence of our specific treatment of the evolution of the angular momentum content. In particular, we have made four crucial assumptions: (i) the specific angular momentum of the baryons is conserved, (ii) the spin parameter of the dark matter haloes is constant with time, (iii) the angular momentum vectors of all mass shells are aligned, and (iv) the baryons and dark matter have the same density and angular momentum distribution

Relaxing assumptions (i) and/or (iii) in general will only worsen the DCP. As discussed in Section 1 conservation of specific angular momentum is required to produce disks with the correct size distribution. Furthermore, gas with misaligned angular momentum vectors has to align itself in order to form a disk, which it can only do by transferring angular momentum to the halo, thus resulting in even more compact disks.

Since disks form from the inside out, one obvious way of preventing too much mass from cooling to small radii is to relax (ii) and assume that the spin parameters of protogalaxies were systematically higher at higher redshift. However, although for each individual halo λ is likely to vary with redshift, such a *systematic* trend with z seems to be ruled out by the fact that N-body simulations have shown that the spin parameter distribution is virtually independent of mass, environment and/or redshift (Lemson & Kauffmann 1999). Analytical studies by Heavens & Peacock (1988) and Catelan & Theuns (1996) have suggested a small anti-correlation between the average spin parameter and the peak height of density fluctuations. However, the amplitude of this correlation is much smaller than the spread in λ at any given value of the peak height, and this effect will thus not significantly affect our results.

We can further check the validity of assumption (ii) by comparing the resulting angular momentum distributions of the dark matter haloes to N-body simulations of structure formation. In a recent paper, Bullock et al. (2000, hereafter B00) have shown that dark matter haloes in a high resolution ΛCDM N-body simulation have specific angular momentum profiles that are well fit by

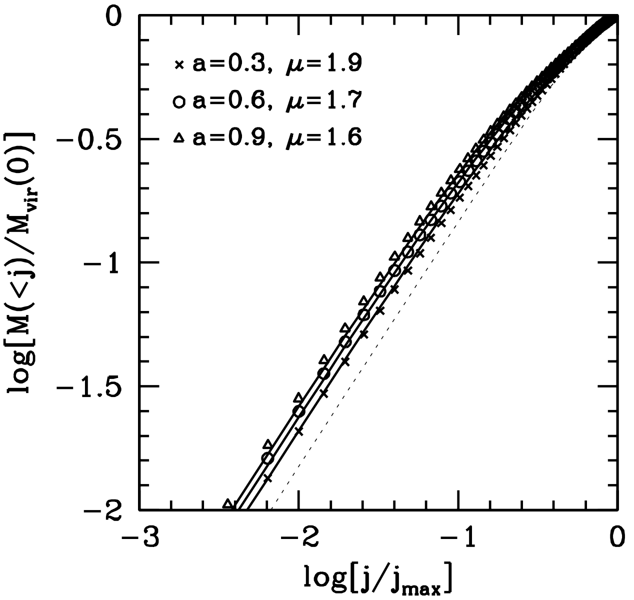

Figure 12. The mass distribution of specific angular momentum for models with $M_{\rm vir}(0) = 5 \times 10^{11} h^{-1}\,{\rm M}_\odot$ and $\lambda = 0.06$. Results are shown for three different MAHs: $a = 0.3$ (crosses), $a = 0.6$ (open circles), and $a = 0.9$ (open triangles). The solid lines are the best fit profiles of the form (31). Shown for comparison is the distribution for a uniform sphere in solid body rotation (thin dotted curve). The best fit values for μ are listed in the figure, and vary from $\mu = 1.6$ ($a = 0.9$) to $\mu = 1.9$ ($a = 0.3$), well in the range of μ values found by B00. This implies that our assumptions regarding the evolution of the angular momentum result in realistic angular momentum profiles.

$$m(j) \equiv \frac{M(<j)}{M_{\rm vir}} = \mu \frac{(j/j_{\rm max})}{(j/j_{\rm max}) + \mu - 1} \tag{31}$$

Here $M(<j)$ is the halo mass with specific angular momentum less than j, $M_{\rm vir}$ is the halo's virial mass, μ is a free parameter, and $j_{\rm max}$ is the maximum specific angular momentum in the halo. B00 have shown that the angular momentum content of a dark matter halo is well described by the pair (λ, μ), and that for 90 percent of the haloes $1.06 < \mu < 2.0$ with a mean of $\langle \mu \rangle = 1.25$. We have computed $m(j)$ for several of our models. The results for three models with $M_{\rm vir}(0) = 5 \times 10^{11} h^{-1}\,{\rm M}_\odot$ are shown in Figure 12, together with the best fit profiles of the form (31). As can be seen, the mass distribution of specific angular momentum in our models is well described by equation (31) with best fit values for μ in the range $1.6 \lesssim \mu \lesssim 1.9$, in good agreement with the results of B00. We have also tested whether μ is correlated with mass, and find a very weak decrease of μ with halo mass[‡], again in good agreement with B00.

Although our best-fit values of μ are well inside the range of μ values found by B00, the spread we obtain is

‡ for $a = 0.6$ we find that μ decreases from 1.76 for $M_{\rm vir}(0) = 5 \times 10^{9} h^{-1}\,{\rm M}_\odot$ to $\mu = 1.68$ for $M_{\rm vir}(0) = 5 \times 10^{12} h^{-1}\,{\rm M}_\odot$

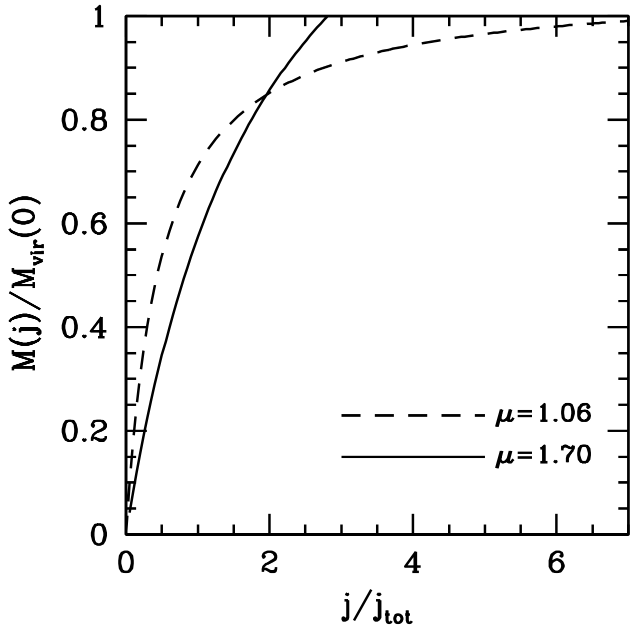

Figure 13. Mass fractions $M(j)/M_{\rm vir}(0)$ as function of $j/j_{\rm tot}$ for two different values of μ. Decreasing μ increases $j_{\rm max}$, and thus the amount of high angular momentum material, and simultaneously increases the amount of low angular momentum material. Lowering μ thus has the same effect as viscosity.

much smaller. However, this is most likely a reflection of the fact that our model haloes have smooth, spherical density distributions without any substructure. This also explains why B00 find a weak correlation between λ and μ, whereas in our models the $m(j)$ profiles are independent of the value of the halo spin parameter. Nevertheless, it is worthwhile to examine whether the DCP can be solved by resorting to haloes with other values of μ. In order to address this issue it is useful to rewrite equation (31) in the form

$$m(j) = \mu \frac{(j/j_{\rm tot})}{(j/j_{\rm tot}) + (\mu - 1)(j_{\rm max}/j_{\rm tot})} \tag{32}$$

Here

$$j_{\rm tot} = \frac{J_{\rm vir}}{M_{\rm vir}} = j_{\rm max}\left(1 - \mu\left[1 - (\mu-1){\rm ln}\left(\frac{\mu}{\mu-1}\right)\right]\right) \tag{33}$$

is the total specific angular momentum of the halo. Substituting equation (33) in (32) one can compute $m(j)$ as function of $j/j_{\rm tot}$ for a given value of μ. Results for $\mu = 1.7$ (the average value found for our haloes) and $\mu = 1.06$ (the 5 percent lower bound of the distribution found by B00) are shown in Figure 13. As is immediately evident, lower values of μ result in higher values of $j_{\rm max}$, and thus in more extended disks. However, at the same time, decreasing μ increases $m(j)$ at low values of $j/j_{\rm tot}$, which implies that the disk will become more centrally concentrated, thus aggravating the DCP. In fact, lowering μ mimics the effects of viscosity (cf. Zhang & Wyse 2000).

It thus becomes clear that in order to solve the DCP it is required that the baryons have an angular momentum distribution that is completely decoupled from that of the dark matter (i.e., assumption (iv) is in error). The baryons need an angular momentum distribution with both less low angular momentum material and more high angular momentum material (i.e., a tail that extends to higher $j_{\rm max}$). From the above it is clear that this can not be realized by merely changing μ. Rather, the baryons need an angular momentum distribution that is completely different from that of equation [31] (see also van den Bosch, Burkert & Swaters 2001).

6 DISCUSSION & CONCLUSIONS

In our current paradigm of galaxy formation, the angular momentum of protogalaxies originates from tidal torques of nearby density perturbations. It has become clear that this mechanism provides just enough angular momentum to produce disk galaxies of the right size (Fall & Efstathiou 1980; Dalcanton et al. 1997; Mo et al. 19998), implying that the baryons can not lose a significant fraction of their specific angular momentum. In the standard picture of disk formation it is therefore assumed that the baryons conserve their specific angular momentum when cooling to form the disk. Under these conditions one can directly compute the density distribution of the resulting disk once the actual distribution of specific angular momentum of the protogalaxy is known.

Recently, Bullock et al. (2000) have determined the specific angular momentum distribution of a large set of dark matter haloes in a ΛCDM universe, and have shown that if baryons have the same angular momentum distribution as dark matter, the resulting disk galaxies are more centrally concentrated than an exponential. This then raises the question whether or not baryonic processes related to star formation, bulge formation, and feedback can produce stellar disks with exponential surface brightness distributions out of such highly concentrated gas disks. In this paper we have presented new models for the formation of disk galaxies to address this question. We use a simple parameterized description of the mass accretion histories of the dark matter haloes, and, following Firmani & Avila-Reese (2000) and Avila-Reese & Firmani (2000), the assumption is made that the halo spin parameter is constant with time. We have shown that this implies specific angular momentum distributions that are in good agreement with those obtained by Bullock et al. (2000) from high resolution N-body simulations. Including cooling and adiabatic contraction, we have confirmed the results of Dalcanton et al. (1997), Firmani & Avila-Reese (2000), and Bullock et al. (2000) that the resulting gas disks are more centrally concentrated than an exponential. Next we included simple prescriptions to describe star formation, bulge formation, feedback, and chemical evolution, and investigated whether these processes can transform the highly concentrated gas disks into stellar disks with close to exponential surface brightness distributions as observed.

At first sight our models are remarkably successful in producing disk galaxies with density distributions as observed. The essential ingredient is bulge formation, which prevents the formation of systems with strongly declining rotation curves. Furthermore, the process of bulge formation results in stellar disks with close to exponential surface brightness profiles. This result is fairly insensitive to the details of the bulge formation process, as long as it is coupled to a stability criterion for the disk (cf. van den Bosch 1998).

The introduction of a star formation threshold density, as motivated by the results of Kennicutt(1989), yields gas mass fractions and stellar truncation radii in excellent agreement with observations (cf. van den Bosch 2000; van den Bosch & Dalcanton 2000).

Despite these clear successes of the model, a closer inspection of the model galaxies reveals two important shortcomings. The first problem mainly concerns LSB disk galaxies. These systems form out of protogalaxies with high angular momentum and do not produce a significant bulge component. This fact that LSB galaxies have typically lower bulge-to-disk ratios than their HSB counterparts is in good agreement with observations. However, the resulting stellar disks of these LSB systems are too centrally concentrated. Although their surface density profiles are close to exponential at the outside, they reveal a strong central cusp in clear disagreement with observations. The second problem concerns the extent of the gas disks. The models predict truncation radii of the gas close to the radii $R_{\rm HI}$ where the HI column density has fallen to $\sim 10^{20}$ cm^{-2}. In real disk galaxies, however, HI is observed out to radii well in excess of $R_{\rm HI}$, again in clear contradiction with the models.

The problem with the truncation radii seems straightforward to solve by including viscosity, which will transport disk mass in the outer parts to larger radii. However, at the same time viscous transport is oriented inwards at small radii. Thus, whereas viscosity seems the obvious solution for the problem with the truncation radii, it will only aggravate the problem with the central concentration of (LSB) disks, and additional processes are required to solve the problems at hand.

Including a simple model for a galactic wind induced by SNe can expel large amounts of baryonic matter from the disk, but it does so with a relative efficiency that is virtually independent of radius. This implies that the actual density distribution is, except for an offset, left intact. Additional energy input from AGNs, not taken into account in our models, is unlikely to solve the problem with the overly concentrated LSB galaxies, since the mass of massive black holes is strongly correlated with that of the bulges, which are virtually absent in LSB galaxies.

Some studies in the past have suggested that LSB galaxies differ from their HSB counterparts in that they form in density peaks of lower amplitude, rather than in peaks with more angular momentum (as assumed here). This implies that LSB galaxies form later and inside haloes of lower densities. By exploring a wide range of MAHs and halo concentrations we have shown that even for this picture the LSB disks are too centrally concentrated.

We therefore conclude that understanding the formation of disk galaxies in CDM cosmologies faces two important challenges. We first of all need a mechanism that can prevent the angular momentum catastrophe which results in disks being an order of magnitude too small. Furthermore, even if the mass accretion is smooth and the angular momentum conserved, the disks that form, although of the right size, are too centrally concentrated. The robustness of this problem seems to suggest that the baryons need an angular momentum distribution that is clearly distinct from that of the dark matter. Similar results were recently obtained by Navarro & Steinmetz (2000) and van den Bosch, Burkert & Swaters (2001). Navarro & Steinmetz used simple scaling relations to show that, in a ΛCDM Universe, disk galaxies only need to accrete a small fraction of the total baryonic mass to match the zero-point of the Tully-Fisher relation, but must draw a comparably much larger fraction of the available angular momentum. Van den Bosch, Burkert & Swaters computed the angular momentum distributions of a sample of low-mass disk galaxies from the observed rotation curves and disk density distributions. A comparison with the angular momentum distributions of cold dark matter haloes found by Bullock et al. (2000), clearly reveals that disks lack predominantly low angular momentum material compared to their dark matter haloes.

An interesting alternative to considering a decoupling between the dark and baryonic mass components, is to change the nature of the dark matter. Recently, numerous studies have focussed on scenarios in which the dark matter is warm (WDM) or self-interacting (SIDM). In both cases one expects dark matter haloes to have constant density cores with less substructure than in CDM models (e.g., Spergel & Steinhardt 2000; Bode, Ostriker & Turok 2001). This not only alleviates the problems with disk rotation curves and the angular momentum catastrophe, but it will also result in disks that are less centrally concentrated. In order to investigate whether a modification of the nature of dark matter might solve the disk concentration problem, we have investigated models in which the haloes have (large) constant density cores. As expected, the resulting disks are more extended as in the CDM case, and with surface brightness profiles that start to approach an exponential form. However, at the same time the disks become more self-gravitating, resulting in the formation of relatively massive bulges. Therefore, the problem of producing bulge-less LSB galaxies with exponential surface brightness profiles remains. Before concluding that the disk concentration problem persists even in WDM and SIDM scenarios, we caution that throughout we have made the assumption that the halo spin parameter does not evolve with time. Although this seems a valid assumption to make in the case of CDM, very little is known about the (evolution) of the angular momentum distribution of haloes in alternative dark matter scenarios. An investigation of the distribution of angular momentum in haloes of warm and/or self-interacting dark matter will proof extremely useful in this context.

ACKNOWLEDGMENTS

I am indebted to Andreas Burkert, Stéphane Charlot, Guinevere Kauffmann, Houjun Mo, and Simon White for stimulating discussions, and to the anonymous referee for insightful comments. Partial support for this work was provided by the National Science Foundation under Grant No. PHY94-07194, and by NASA through Hubble Fellowship Grant No. HF-01102.11-97.A awarded by the Space Telescope Science Institute, which is operated by AURA for NASA under contract NAS 5-26555.

REFERENCES

Andredakis Y.C., Peletier R.F., Balcells M., 1995, MNRAS, 275, 874

Avila-Reese V., Firmani C., Hernández X., 1998, ApJ, 505, 37

Avila-Reese V., Firmani C., 2000, RevMexAA, 36, 23
Barnes J.E., Efstathiou G., 1987, ApJ, 319, 575
Barteldrees A., Dettmar R.-J., 1994, A&AS, 103, 475
Begeman K.C., 1989, A&A, 233, 47
Bland-Hawthorn J., Freeman K.C., Quinn P.J., 1997, ApJ, 490, 143
Blumenthal G.R., Faber S.M., Flores R., Primack, J.R., 1986, ApJ, 301, 27
Bode P., Ostriker J.P., Turok N., 2000, preprint (astro-ph/0010389)
Bryan G., Norman M., 1998, ApJ, 495, 80
Bruzual G.A., Charlot S., 1993, ApJ, 405, 538
Buchalter A., Jimenez R., Kamionkowski M., 2001, MNRAS, 322, 43
Bullock J.S., Dekel A., Kolatt T.S., Kravtsov A.V., Klypin A.A., Porciani C., Primack J.R., 2000, preprint (astro-ph/0011001), (B00)
Bullock J.S., Kolatt T.S., Sigad Y., Somerville R.S., Klypin A.A., Primack J.R., Dekel A., 2001, MNRAS, 321, 559
Carignan C., Beaulieu S., 1989, ApJ, 347, 760
Carignan C., Puche D., 1990a, AJ, 100, 641
Carignan C., Puche D., 1990b, AJ, 100, 394
Catelan P., Theuns T., 1996, MNRAS, 282, 436
Christodoulou D.M., Shlosman I., Tohline J.E., 1995, ApJ, 443, 551
Clarke C.J., 1989, MNRAS, 238, 283
Cole S., Lacey S., 1996, A&A, 281, 716
Côté S., Carignan C., Sancisi R., 1991, AJ, 102, 904
Crampin D.J., Hoyle F., 1964, ApJ, 140, 99
Dalcanton J.J., Spergel D.N., Summers F.J., 1997, ApJ, 482, 659
de Blok W.J.G., van der Hulst J.M., Bothun G.D., 1995, MNRAS, 274, 235
de Grijs R., Kregel M., Wesson K.H., 2001, MNRAS, 324, 1074
de Jong R.S., 1996, A&A, 313, 377
de Jong R.S., Lacey C., 2000, ApJ, 545, 781
Domínguez-Tenreiro R., Tissera P.B., Sáiz A., 1998, ApJ, 508, 123
Efstathiou G., 2000, MNRAS, 317, 697
Eke V.R., Efstathiou G., Wright L., 2000, MNRAS, 315, 18
Fall S.M., Efstathiou G., 1980, MNRAS, 193, 189
Ferguson A.M.N., Clarke C.J., 2001, MNRAS, 325, 781
Ferrarese L., Merritt D., 2000, ApJ, 539, 9
Firmani C., Tutukov A.V., 1994, A&A, 288, 713
Firmani C., Avila-Reese V., 2000, MNRAS, 315, 457
Flores R., Primack J.R., Blumenthal G.R., Faber S.M., 1993, ApJ, 412, 443
Flores R., Primack J.R., 1994, ApJ, 427, L1
Fukushige T., Makino J., 1997, ApJ, 477, L9
Gebhardt K. et al., 2000, ApJ, 539, 13
Gerola H., Seiden P.E., 1978, ApJ, 223, 129
Heavens A.F., Peacock J., 1988, MNRAS, 232, 339
Heavens A.F., Jimenez R., 1999, MNRAS, 305, 770
Hernquist L., 1990, ApJ, 356, 359
Jimenez R., Padoan P., Matteucci F., Heavens A.F., 1998, MNRAS, 296, 1089
Jing Y.P., 2000, ApJ, 535, 30
Jobin M., Carignan C., 1990, AJ, 100, 648
Kamionkowski M., Liddle A.R., 2000, Phys. Rev. Let. 84, 4525
Kauffmann G., 1996, MNRAS, 281, 475
Kauffmann G., White S.D.M., Guiderdoni B., 1993, MNRAS, 264, 201
Kennicutt R.C.Jr., 1989, ApJ, 344, 685
Kennicutt R.C.Jr., 1998, ApJ, 498, 541
Kormendy J., Richstone D., 1995, ARA&A, 33, 581
Lacey C., Cole S., 1993, MNRAS, 262, 627
Lemson G., Kauffmann G., 1999, MNRAS, 302, 111
Lin D.N.C., Pringle J.E., 1987, ApJ, 320, 87L
Maloney P., 1993, ApJ, 414, 41
McGaugh S.S., Bothun G.D., 1994, AJ, 107, 530
McGaugh S.S., de Blok W.J.G., 1998, ApJ, 499, 41
Mestel L., 1963, MNRAS, 126, 553
Mo H.J., McGaugh S.S., Bothun G.D., 1994, MNRAS, 267, 129
Mo H.J., Mao S., White S.D.M., 1998, MNRAS, 295, 319
Moore B., 1994, Nature, 370, 629
Moore B., Governato F., Quinn T., Stadel J., Lake G., 1998, ApJ, 499, L5
Mushotzky R., Loewenstein M., 1997, ApJ, 481, 63
Natarajan P., 1999, ApJ, 512, 105
Navarro J.F., Benz W., 1991, ApJ, 380, 320
Navarro J.F., Frenk C.S., White S.D.M., 1996, ApJ, 462, 563
Navarro J.F., Frenk C.S., White S.D.M., 1997, ApJ, 490, 493
Navarro J.F., Steinmetz M., 1997, ApJ, 478, 13
Navarro J.F., Steinmetz M., 1999, ApJ, 513, 555
Navarro J.F., Steinmetz M., 2000, ApJ, 538, 477
Olivier S.S., Blumenthal G.R., Primack J.R., 1991, MNRAS, 252, 102
Pickering T.E., Impey C.D., van Gorkum J.H., Bothun G.D., 1997, AJ, 114, 1858
Pohlen M., Dettmar R.-J., Lütticke R., 2000, A&A, 357, 1P
Puche D., Carignan C., van Gorkum J.H., 1991, AJ, 101, 456
Romanishin W.E., Strom K.M., Strom S.E., 1983, ApJS, 53, 105
Ryden B.S., 1988, ApJ, 329, 589
Scalo J.N., 1986, Fundam. Cosmic Phys., 11, 1
Schmidt M., 1959, ApJ, 129, 243
Seiden P.E., Schulman L.S., Elmegreen B.G., 1984, ApJ, 282, 95
Silk J., 1997, ApJ, 481, 703
Sommer-Larsen J., Gelato S., Vedel H., 1999, ApJ, 519, 501
Sommer-Larsen J., Dolgov A., 2001, ApJ, 551, 608
Spergel D.N., Steinhardt P.J., 2000, Phys. Rev. Let., 84, 17
Sprayberry D., Impey C.D., Bothun G.D., Irwin M.J., 1995, AJ, 109, 558
Sunyaev R.A., 1969, Astrophys. Letters , 3, 33
Sutherland R., Dopita M., 1993, ApJS, 88, 253
Swaters R.A., 1999, PhD Thesis, University of Groningen, The Netherlands
Tan J.C., 2000, ApJ, 536, 173
Toomre A., 1964, ApJ, 139, 1217
Tóth G., Ostriker J.P., 1992, ApJ, 389. 5
Tytler D., Burles S., Lu L., Fan X.-M., Wolfe A., Savage, B., 1999, AJ, 117, 63
van den Bosch F.C., 1998, ApJ, 507, 601
van den Bosch F.C., 2000, ApJ, 530, 177
van den Bosch F.C., Dalcanton J.J., 2000, ApJ, 534, 146
van den Bosch F.C., Robertson B.E., Dalcanton J.J., de Blok W.J.G., 2000, AJ, 119, 1579
van den Bosch F.C., Swaters R.A., 2001, MNRAS, 325, 1017
van den Bosch F.C., Burkert A., Swaters R.A., 2001, MNRAS, in press (astro-ph/0105082)
van der Kruit P.C., Searle L., 1981a, A&A, 95, 105
van der Kruit P.C., Searle L., 1981b, A&A, 95, 116
Warren M.S., Quinn P.J., Salmon J.K., Zurek W.H., 1992, ApJ, 399, 405
Weil M.L., Eke V.R., Efstathiou G., 1998, MNRAS, 300, 773
White S.D.M., Rees M.J., 1978, MNRAS, 183, 341
White S.D.M., Navarro J.F., 1993, MNRAS, 265, 271
Wyse R.F.G., 1986, ApJ, 311, L41
Wyse R.F.G., Silk J., 1989, ApJ, 339, 700
Yoshii Y., Sommer-Larsen J., 1989, MNRAS, 236, 779
Zhang B., Wyse R.F.G., 2000, MNRAS, 313, 310